

# Verifying detailed fluctuation relations for discrete feedback-controlled quantum dynamics

Patrice A. Camati<sup>1,\*</sup> and Roberto M. Serra<sup>1,2,†</sup>

<sup>1</sup>*Centro de Ciências Naturais e Humanas, Universidade Federal do ABC,  
Avenida dos Estados 5001, 09210-580 Santo André, São Paulo, Brazil*

<sup>2</sup>*Department of Physics, University of York, York YO10 5DD, United Kingdom*

Discrete quantum feedback control consists of a managed dynamics according to the information acquired by a previous measurement. Energy fluctuations along such dynamics satisfy generalized fluctuation relations, which are useful tools to study the thermodynamics of systems far away from equilibrium. Due to the practical challenge to assess energy fluctuations in the quantum scenario, the experimental verification of detailed fluctuation relations in the presence of feedback control remains elusive. We present a feasible method to experimentally verify detailed fluctuation relations for discrete feedback control quantum dynamics. Two detailed fluctuation relations are developed and employed. The method is based on a quantum interferometric strategy that allows for the verification of fluctuation relations in the presence of feedback control. An analytical example to illustrate the applicability of the method is discussed. The comprehensive technique introduced here can be experimentally implemented at a microscale with the current technology in a variety of experimental platforms.

## I. INTRODUCTION

Feedback control is a process which allows the control of the system dynamics based on information of its present or past states. Maxwell pioneered the mathematical analysis of control systems in the second half of the 19th century [1, 2]. Due to the growing application of automation in industry, control theory plays a major role in modern engineering and technology [3], e.g., using feedback control for stabilization of dynamical systems. Feedback control has also been used to control quantum systems, e.g., for reducing unwanted noise [4, 5]. Maxwell's demon, an important thought experiment envisaged by Maxwell [6–8], may also be recognized as a feedback control protocol at the microscopic scale. Along with the work of Jaynes [9, 10] concerning the informational character of statistical mechanics, they comprise prominent examples of the interplay between information theory and thermodynamics.

One approach to study the nonequilibrium thermodynamics of small quantum systems is based on fluctuation relations [11–15]. Quantities such as work, heat, and entropy production are described by stochastic variables and establish deep relations between nonequilibrium and equilibrium thermodynamic quantities [16, 17]. The Jarzynski equality [18, 19] and Crooks relation [20] connect the nonequilibrium work with the equilibrium free-energy difference. Despite their classical origin, their validity has been extended to driven quantum systems [21–25]. These fundamental relations were also extended for feedback protocols, providing further tools to study information thermodynamics of classical and quantum systems [32–45]. They imply generalized forms of the

second law where thermodynamic and information quantities are treated on an equal footing [46–52]. There are a few qualitatively different generalized second laws in the presence of feedback control, involving the information gain [53–59], the mutual information [60], or even the entanglement of formation [61].

From the experimental point of view, quantum fluctuation relations have been tested very recently in a nuclear magnetic resonance (NMR) quantum processor [26, 27], employing interferometric methods [62, 63], and in a trapped-ions setup [28]. In classical information thermodynamics, the extension of the Jarzynski relation [64], the Landauer's principle [65], the Szilard engine [66–68], and Maxwell's demon [69, 70] have been performed experimentally. On the other hand, in quantum information thermodynamics [71] there has been little experimental activity in the past couple of years, due to the inherent difficulties associated to the quantum setup. Chronologically, information-to-energy conversion [72] and Maxwell's demon [59] have been accomplished in an NMR quantum processor; a photonic architecture was employed to address the minimum entropy cost necessary for the implementation of a quantum measurement [73]; communication-assisted games based on a logical version of Maxwell's demon provided an entanglement-separability criterion in multiphoton optical interferometers [74]; another realization of Maxwell's demon has been done in both the classical and quantum regimes in circuit quantum electrodynamics (QED) [75]; the experimental verification of the integral fluctuation relation in the presence of feedback control was very recently implemented both encompassing absolute irreversibility performing nondemolition quantum measurements [76] and encompassing inefficient measurements employed by continuous weak measurements [77] using transmon qubits in circuit QED.

The integral fluctuation relation for feedback-controlled systems has been obtained for two different

\* [p.camati@ufabc.edu.br](mailto:p.camati@ufabc.edu.br)

† [serra@ufabc.edu.br](mailto:serra@ufabc.edu.br)

physical scenarios. In the first, the quantum system is controlled by a noisy classical feedback device which introduces a control mismatch between the observable measurement basis and the feedback control basis. In this situation, the mutual information (density) between the measurement and the feedback control appears in the integral fluctuation relation [49]. This setting assumes that the controller implements the measurement of an observable, i.e., a projective measurement. On the other hand, another setting was developed in Ref. [52] in which an auxiliary quantum system is employed to implement a controller which performs an inefficient positive operator-valued measure (POVM). In this case, the information gain (density) of the measurement appears in the integral fluctuation relation. We note that these settings are physically distinct, since the information-theoretic quantity in the first setting is present due to a (classical) noisy controller, while in the second setting it comes from the inefficient POVM measurement performed by the controller.

The detailed fluctuation relation for feedback control characterizes the irreversibility in controlled systems and is a generalization of the integral fluctuation relations. For the first setting mentioned above, with a noisy controller, the detailed fluctuation relation was obtained in Ref. [51]. Up to the present moment, the detailed fluctuation relation for feedback control has not been experimentally verified either in the classical or in the quantum scenario. Here we propose a method to experimentally assess the statistics of energy fluctuations which allows the verification of the quantum detailed fluctuation relation for processes driven by discrete-time feedback control. The method is based on interferometric protocols that can be put into action with the current technology in a variety of experimental platforms.

This paper is organized as follows. In Sec. II we review the definition of a backward process using the time-reversal operator. In Sec. III we employ this formalism to review the detailed fluctuation relations with and without feedback control. We show that they remain valid without assuming time-reversal invariance, which is usually assumed in the literature. Furthermore, we derive two detailed fluctuation relations which are instrumental in our method. One applies to feedback without control mismatch, whereas the other applies to feedback with control mismatch. In Sec. IV we present a method to experimentally verify the detailed fluctuation relation for discrete feedback-controlled quantum dynamics. The method uses the detailed fluctuation relations for single histories and five quantum interferometric circuits. To illustrate our method, we study the analytical example of a qubit controlled by conditional sudden quenches in Sec. V. We summarize in Sec. VI.

## II. TIME-REVERSAL TRANSFORMATION AND THE DEFINITION OF BACKWARD PROCESSES

Detailed fluctuation relations involve the forward and backward probability density functions (PDFs) of a protocol. In order to properly discuss the backward process, we shortly review the formalism of the time-reversal operator. In the next section we show that the quantum detailed fluctuation relations (QDFRs) apply for systems without time-reversal symmetry. This contrasts with some previous approaches where the system dynamics was restricted to be time-reversal symmetric. We note that a few authors have also realized this fact [78?–81].

In quantum mechanics, symmetry operations have to preserve probabilities, which, in turn, are based on inner products. This necessary condition implies that a symmetry operator  $\mathcal{O}$  must satisfy  $|(\mathcal{O}|\psi\rangle, \mathcal{O}|\varphi\rangle)| = |(|\psi\rangle, |\varphi\rangle)|$ , where  $(\cdot, \cdot)$  is the Hilbert space inner product (here we assume the first entry to be antilinear and the second one to be linear). Wigner showed that any symmetry operator is given by either a unitary or antiunitary operator [82]. By definition, unitary operators leave the inner product invariant,  $(\mathcal{O}|\psi\rangle, \mathcal{O}|\varphi\rangle) = (|\psi\rangle, |\varphi\rangle)$ , whereas antiunitary operators induce a conjugation,  $(\mathcal{O}|\psi\rangle, \mathcal{O}|\varphi\rangle) = (|\psi\rangle, |\varphi\rangle)^* = (|\varphi\rangle, |\psi\rangle)$ . The application of antilinear operators is subtle and the interested reader may find Refs. [83–85] helpful.

The usual symmetry operations, such as translations or rotations in space, acquire a unitary representation. These operations can be implemented in the laboratory by either a change of reference frame or a physical position of the experimental setting (passive and active coordinate transformations, respectively). On the other hand, the time-reversal and charge-conjugation operators are two well-known antiunitary symmetries and they cannot be implemented either by a change of reference frame or by a change in the physical setup. Therefore, to experimentally access the time-reversal symmetry, two different, but otherwise related, experiments should be performed. These two related processes are called forward and backward and how they are related to each other will be discussed below. In the quantum case, the system is time-reversal symmetric when the mathematical condition  $[H(t), \Theta] = 0$  is satisfied, where  $H(t)$  is a time-dependent Hamiltonian for a driven system and  $\Theta$  is the time-reversal operator. For our purposes, the most interesting cases comprise dynamics which are not time-reversal symmetric, such as a spin-1/2 particle driven by an external magnetic field as in the experiments reported in Refs. [26, 27].

Let  $|\psi(t)\rangle$  be the solution of the Schrödinger equation for a time-dependent Hamiltonian  $H(t)$ , driven by some external parameter, with the initial condition  $|\psi_0\rangle$  at  $t = 0$ . Suppose that the total time length for this driven protocol is  $\tau$ . This dynamics is called the forward process. The final state of the forward evolution will be  $|\psi_\tau\rangle$  at  $t = \tau$ . If we apply the time-reversal op-

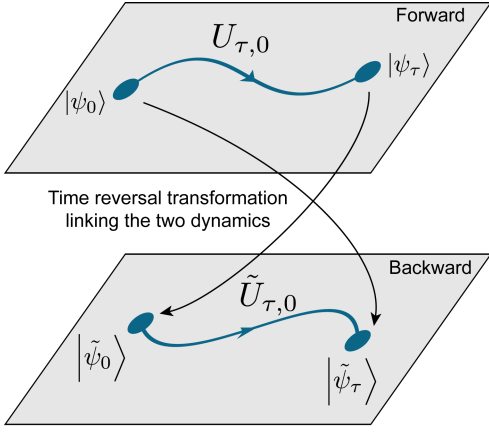


Figure 1. Representation of the forward and backward processes. The two planes represent two parts of the system Hilbert space. The forward and backward trajectories are mapped by the time-reversal transformation. We emphasize that from the practical point of view, there are two physically distinct experiments, one for each history. Each evolution runs forward in time and both are precisely connected by the time-reversal transformation for any given time  $t \in [0, \tau]$ .

erator  $\Theta$  and change the time counting as  $t \rightarrow \tau - t$  in the Schrödinger equation of the forward process a new Schrödinger equation is obtained

$$i\hbar \frac{d}{dt} |\tilde{\psi}(t)\rangle = \tilde{H}(t) |\tilde{\psi}(t)\rangle, \quad (1)$$

with  $|\tilde{\psi}(t)\rangle = \Theta |\psi(\tau - t)\rangle$  and  $\tilde{H}(t) = \Theta H(\tau - t) \Theta^\dagger$ . The reverse protocol described by Eq. (1) with the initial condition  $|\tilde{\psi}_0\rangle = \Theta |\psi_\tau\rangle$  is called the backward process (see Fig. 1).

The evolution operators for the backward and forward processes are also related to each other. For a nondegenerate discrete Hamiltonian, the eigenequation of the forward process is  $H(t) \Pi_n^t = E_n^t \Pi_n^t$ , where  $E_n^t$  and  $\Pi_n^t = |E_n^t\rangle \langle E_n^t|$  are the instantaneous eigenvalues and eigenprojectors, respectively. Correspondingly, the eigenequation for the backward process is given by  $\tilde{H}(t) \tilde{\Pi}_n^t = \tilde{E}_n^t \tilde{\Pi}_n^t$ , where  $\tilde{E}_n^t = E_n^{\tau-t}$  and  $\tilde{\Pi}_n^t = \Theta \Pi_n^{\tau-t} \Theta^\dagger$  are the instantaneous eigenvalues and eigenprojectors of the time-reversed dynamics, respectively. Furthermore, the evolution operator for the forward process is  $U_{\tau,0} = \mathcal{T}_> \exp \left\{ -\frac{i}{\hbar} \int_0^\tau dt H(t) \right\}$ , where  $\mathcal{T}_>$  is the time-ordering operator. Using the time-reversal transformations, one can show that

$$\begin{aligned} \Theta U_{\tau,0} \Theta^\dagger &= \mathcal{T}_> \exp \left\{ -\frac{i}{\hbar} \int_\tau^0 dt \Theta H(\tau - t) \Theta^\dagger \right\} \\ &= \tilde{U}_{\tau,0}^\dagger. \end{aligned} \quad (2)$$

Sometimes this relation is interpreted as follows: The evolution operator of the forward process between times

0 and  $\tau$  is mapped to the evolution operator of the backward process between times  $\tau$  and 0; thus, time would run backward.

### III. QUANTUM DETAILED NONEQUILIBRIUM FLUCTUATION RELATIONS

#### A. Without feedback control

In the light of the formalism introduced in the preceding section, we review the derivation of the QDFR without feedback and show that it remains valid for a dynamics which is not symmetric under time reversal. The QDFR applies to the following scenario. A system starts in thermal equilibrium in the initial Gibbs state  $\rho_0^{eq} = e^{-\beta H_0} / Z_0$  with initial Hamiltonian  $H_0$ , inverse temperature  $\beta = (k_B T)^{-1}$ , and partition function  $Z_t = \text{Tr} [e^{-\beta H_t}]$ , where  $k_B$  is the Boltzmann constant. The system is driven away from equilibrium due to the manipulation of controllable parameters in the Hamiltonian, for instance, the external magnetic field. The protocol occurs during a time length  $\tau$  which drives the system to the final state  $\rho_\tau = U_{\tau,0} \rho_0^{eq} U_{\tau,0}^\dagger$ . For this process, the first law of thermodynamics requires the equality between the system internal energy difference and the average work,  $\Delta \mathcal{U} = \langle W \rangle$ , with  $\mathcal{U}_t = \text{Tr} [\rho_t H_t]$  being the instantaneous internal energy. The average work is obtained as the average of the (forward) work PDF,  $\langle W \rangle = \int dW W P_F(W)$ , where  $P_F(W)$  is the work PDF associated with the (forward) protocol just described. The work PDF  $P_F(W)$  can be obtained through the two-point measurement (TPM) scheme and is given by [23, 86]

$$P_F(W) = \sum_{m,n} p(m,n) \delta[W - W_{mn}], \quad (3)$$

where

$$\begin{aligned} p(m,n) &= p(m|n) p(n) \\ &= \text{Tr} [\Pi_m^\tau U_{\tau,0} \Pi_n^0 U_{\tau,0}^\dagger] \text{Tr} [\Pi_n^0 \rho_0^{eq}] \end{aligned} \quad (4)$$

is the joint probability distribution of obtaining energy outcomes  $E_m^\tau$  and  $E_n^0$  in the final and initial times, respectively,  $p(m|n)$  is the conditional probability of obtaining the energy outcome  $E_m^\tau$  given that  $E_n^0$  was obtained in the first measurement,  $p(n)$  is the initial probability to obtain  $E_n^0$ , and  $W_{mn} = E_m^\tau - E_n^0$  is the value of work in this system history.

Using the relations obtained in the preceding section between forward and backward processes, one can obtain the QDFR [21, 22] (see APPENDIX A)

$$\frac{P_F(W)}{P_B(-W)} = e^{\beta(W - \Delta F)}, \quad (5)$$

where  $\Delta F = F_\tau - F_0$  is the free-energy difference, with  $F_t = -(\beta)^{-1} \ln Z_t$ , and

$$P_B(W) = \sum_{n,m} \tilde{p}(n,m) \delta[W - \tilde{W}_{nm}] \quad (6)$$

is the work PDF associated with the backward process,  $\tilde{p}(n,m) = \tilde{p}(n|m)\tilde{p}(m)$  is the joint probability distribution of obtaining energy outcomes  $\tilde{E}_n^\tau$  and  $\tilde{E}_m^0$  at the end and beginning of the driven process, respectively,  $\tilde{p}(n|m) = \left| \left\langle \tilde{E}_n^\tau \left| \tilde{U}_{\tau,0} \right| \tilde{E}_m^0 \right\rangle \right|^2$  is the conditional probability of obtaining the energy outcome  $\tilde{E}_n^\tau$  given that  $\tilde{E}_m^0$  was obtained in the first measurement,  $\tilde{p}(m) = e^{-\beta \tilde{E}_m^0} / \tilde{Z}_0$  is the initial probability to obtain  $\tilde{E}_m^0$ , and  $\tilde{W}_{nm} = \tilde{E}_n^\tau - \tilde{E}_m^0$  is the value of work. Our calculation is structurally similar to the others in the literature [21, 22, 87–93]. The distinction of our approach is that the Hamiltonian can be completely arbitrary, time-reversal symmetric, or otherwise. This has both conceptual and practical important consequences, which are discussed in the example below.

Consider the Zeeman Hamiltonian  $H = -\boldsymbol{\mu} \cdot \mathbf{B}(t)$  for a single spin-1/2 particle in a driven magnetic field. In this case the time-reversal operator satisfies  $\Theta^2 = -\mathbb{1}$ , where  $\mathbb{1}$  denotes the identity operator. For such a system, a time-reversal symmetric Hamiltonian has a twofold degeneracy called Kramer's degeneracy [85], i.e., if  $|E_n\rangle$  is an eigenvector then so is  $\Theta|E_n\rangle$  with same eigenenergy  $E_n$ .

Occasionally in the literature [16, 23, 88], in addition to the sign change of the spin operator, the time-reversal transformation is assumed to change the sign of the magnetic field as well. If that were the case, then the Zeeman Hamiltonian would be time-reversal symmetric. This imposed change in the sign of the magnetic field is artificial, though. If the Zeeman Hamiltonian were time-reversal symmetric, then Kramer's degeneracy would imply a spectrum of a single eigenenergy. This would further imply a trivial work PDF, for a driving spin-1/2, given by a single delta function at  $W = 0$ . In Ref. [26] the work PDF for this system was experimentally obtained and the result is not such a trivial PDF.

This argument entails that the Zeeman Hamiltonian is not symmetric under the time-reversal transformation. The (external) magnetic field is not a property of the system and therefore should not change sign under the time-reversal transformation. Mathematically, the time-reversal operator acts on complex numbers, inducing a conjugation, and other operators, states, or observables. As the magnetic field is a real vector it does not change under the time-reversal transformation. However, as we discuss in Sec. V, the magnetic-field direction can be used to effectively implement the backward Hamiltonians in an experimental setting [26].

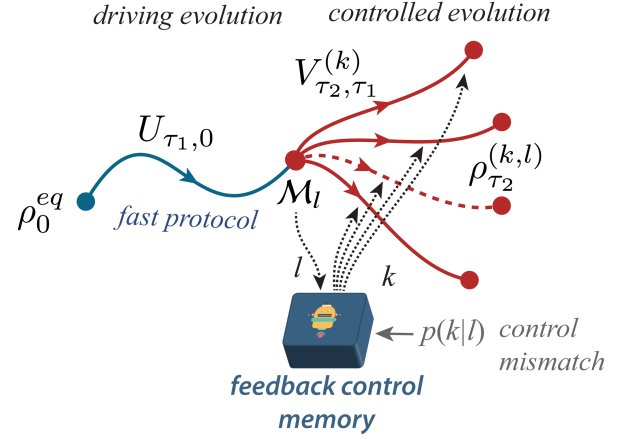


Figure 2. Representation of the forward feedback control protocol. The system starts in a thermal equilibrium state  $\rho_0^{eq}$  and is driven by external means to the nonequilibrium state  $\rho_{\tau_1}$ . An intermediate measurement of some observable  $\mathcal{M}$  is performed at time  $\tau_1$ . The eigenprojectors of the observable are denoted by  $\{\mathcal{M}_l\}$  and the outcome  $l$  is obtained with probability  $p(l)$ . After the measurement, there might be a misimplementation of the feedback control, i.e., the feedback operation associated with outcome  $k$ ,  $V_{\tau_2, \tau_1}^{(k)}$ , is implemented when the actual measurement outcome is  $l$ . This mismatch may occur due to an error or nonideality in the feedback control memory. This is modeled by the conditional probability distribution  $p(k|l)$ . For each possible outcome  $l$  there will be  $k$  different histories for the system. Each of the  $(k, l)$  histories lead to the final state  $\rho_{\tau_2}^{(k,l)}$ , with joint probability  $p(k, l)$ , and final Hamiltonian  $H_{\tau_2}^{(k)}$ , with probability  $p(k)$ .

## B. With Feedback Control

Although the QDFR for feedback processes was discussed in Ref. [51], it was not treated in a way which is clearly experimentally accessible. Hitherto, even in the classical scenario, the generalization of the Crooks relation for feedback processes has not been tested experimentally. We recast the discussion in the light of the approach developed in Sec. II revisiting the derivation of the QDFR in the presence of feedback control as well as introducing two other QDFRs. In the next section we use the results developed here to present a method to experimentally access energy fluctuations and verify the QDFR in the presence of feedback control.

The forward process in the presence of feedback control, illustrated in Fig. 2, is defined in a similar way to the forward process without feedback. The system begins in the Gibbs state  $\rho_0^{eq}$  and is driven away from equilibrium by the evolution  $U_{\tau_1,0}$  up to time  $\tau_1$ ,  $\rho_{\tau_1} = U_{\tau_1,0} \rho_0^{eq} U_{\tau_1,0}^\dagger$ . At this time an intermediate measurement of some observable  $\mathcal{M}$  is performed, leading to the postmeasurement state  $\rho_{\tau_1}^{(l)} = \mathcal{M}_l \rho_{\tau_1} \mathcal{M}_l / p(l)$  with probability  $p(l) = \text{Tr}[\mathcal{M}_l \rho_{\tau_1}]$ , where  $\{\mathcal{M}_l\}$  are the observable eigenprojectors.

After the measurement, a noisy controller implements



the feedback. The feedback operation, described by the unitary operator  $V_{\tau_2, \tau_1}^{(k)}$ , is applied up until time  $\tau_2$ . Note that the index of the feedback operation  $k$  is different from the index of the postmeasurement states  $l$ . This is due to the noisy feature of the controller, which implements the feedback operator  $V_{\tau_2, \tau_1}^{(k)}$  to  $\rho_{\tau_1}^{(l)}$  with conditional probability  $p(k|l)$ . This probability quantifies the control mismatch of the feedback implementation of  $V_{\tau_2, \tau_1}^{(k)}$ , associated with outcome  $k$ , and the actual measurement outcome  $l$ . The control mismatch encompasses possible failures and imperfections in the feedback mechanism.

We denote the instantaneous eigenvalues and eigenprojectors of the  $k$ th feedback Hamiltonian as  $H_t^{(k)} P_m^{(k)t} = E_m^{(k)t} P_m^{(k)t}$ . We note that, rigorously, we should write the indices as  $m = m^{(k)}$  since for each of the  $k$ th Hamiltonians there are  $m^{(k)}$  possible eigenvalues. We have chosen the compact notation in almost all of our expressions for the sake of readability. After the measurement, there will be a number of possible histories for the system, quantified by the product of the indices  $kl$ . Each  $(k, l)$  history will lead to the final state  $\rho_{\tau_2}^{(k, l)} = V_{\tau_2, \tau_1}^{(k)} \rho_{\tau_1}^{(l)} V_{\tau_2, \tau_1}^{(k)\dagger}$ , with joint probability  $p(k, l) = p(k|l)p(l)$ , and the final Hamiltonian  $H_{\tau_2}^{(k)}$ , with probability  $p(k) = \sum_l p(k, l)$ .

Due to the control mismatch, the mutual information density (between the measurement and the controlled evolution) can be introduced [49] and it is given by  $I^{(k, l)} = \ln p(k|l)/p(k)$ , where  $p(k)$  is the probability that the feedback operation  $V_{\tau_2, \tau_1}^{(k)}$  is implemented. The mutual information is given by the average of its density,  $\langle I \rangle = \sum_{k, l} p(k, l) I^{(k, l)}$ , and quantifies the correlation between the measurement and controlled evolution.

The mutual information is a fundamental quantity in information theory [60] and it appears explicitly in one of the generalized forms of the second law in the presence of feedback,  $\langle \Sigma \rangle = \beta (\langle W \rangle - \langle \Delta F \rangle) \geq -\langle I \rangle$ , where the lower bound for the mean entropy production  $\langle \Sigma \rangle$  is a negative quantity [49]. This inequality reveals that the feedback control can be used to rectify the mean entropy production in a nonequilibrium quantum dynamics [59].

We introduce the forward mixed joint PDF for a single system history  $(k, l)$ ,

$$P_F(k, l; W, \Delta F, I) = \sum_{m, n} p(m^{(k)}, k, l, n) \times \delta[W - W_{mkn}] \delta[\Delta F - \Delta F^{(k)}] \times \delta[I - I^{(k, l)}], \quad (7)$$

where  $W_{mkn} = E_m^{(k)\tau_2} - E_n^0$  is the work in the TPM scheme and  $\Delta F^{(k)} = F_{\tau_2}^{(k)} - F_0$  is the free-energy difference associated with the final Hamiltonian  $H_{\tau_2}^{(k)}$ . This mixed PDF encompasses all statistical information of the forward protocol (see APPENDIX B). It contains two discrete variables,  $k$  and  $l$ , and three continuous stochastic variables,  $W$ ,  $\Delta F$ , and  $I$ . In

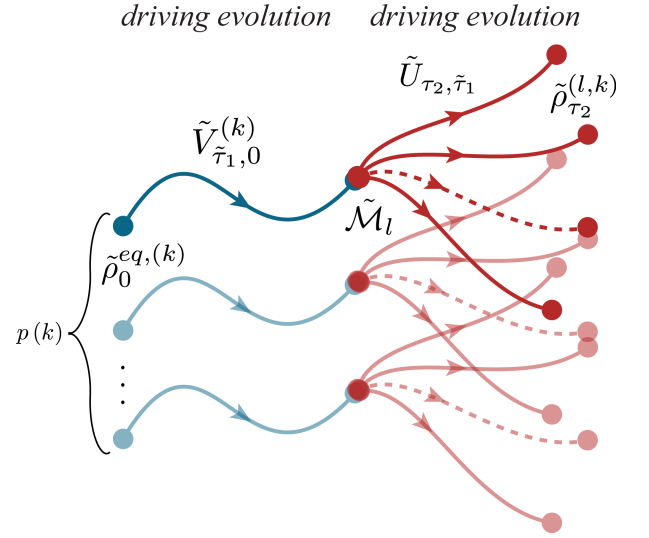


Figure 3. Schematic representation of the backward feedback control protocol. The initial thermal state for the backward protocol  $\tilde{\rho}_0^{eq, (k)} = e^{-\beta \tilde{H}_0^{(k)}} / \tilde{Z}_0$  (where  $\tilde{Z}_t = \text{Tr} e^{-\beta \tilde{H}_t^{(k)}}$ ) is sampled with the probability  $p(k)$  that the associated final Hamiltonian of the forward protocol  $H_{\tau_2}^{(k)}$  occurs. The first driven evolution is conditioned to the corresponding feedback operation in the forward process. For each sampled initial state the appropriate evolution corresponding to the time-reversed Hamiltonian  $\tilde{H}_t^{(k)} = \Theta H_{\tau_2-t}^{(k)} \Theta^\dagger$  from 0 to  $\tilde{\tau}_1 = \tau_2 - \tau_1$  should be implemented. The measurement of the time-reversed observable  $\tilde{\mathcal{M}}$  is performed at time  $\tilde{\tau}_1$ . The set of measurement eigenprojectors is represented by  $\{\tilde{\mathcal{M}}_l\}$  and the outcome  $l$  occurs with probability  $\tilde{p}(l|k)$ . The conditioning in  $k$  is due to the fact that for each initial state, labeled by  $k$ , the measurement probabilities will be different. The final state is designated by  $\tilde{\rho}_{\tau_2}^{(l, k)}$ .

Eq. (7),  $p(m^{(k)}, k, l, n) = p(m^{(k)}|l)p(k|l)p(l|n)p(n)$  is a function of the set of labels  $(m^{(k)}, k, l, n)$ , with  $p(m^{(k)}|l) = \text{Tr} [P_m^{(k)\tau_2} V_{\tau_2, \tau_1}^{(k)} \mathcal{M}_l V_{\tau_2, \tau_1}^{(k)\dagger}]$  the probability of obtaining  $E_m^{(k)\tau_2}$  in the final energy measurement given that the feedback measurement outcome was  $l$ ,  $p(l|n) = \text{Tr} [\mathcal{M}_l U_{\tau_1, 0} P_n^0 U_{\tau_1, 0}^\dagger]$  the probability of obtaining the outcome  $l$  in the feedback measurement given that the initial energy outcome was  $E_n^0$ , and  $p(n) = e^{-\beta E_n^0} / Z_0$  the probability of obtaining the energy outcome  $E_n^0$  in the first measurement. Integrating some variables, we can obtain marginal probability distributions associated with the protocol (see APPENDIX B). In particular, a useful quantity in our method is the mixed work PDF

$$P_F(k, l; W) = \sum_{m, n} p(m^{(k)}, k, l, n) \delta[W - W_{mkn}], \quad (8)$$

which is obtained from Eq. (7) by integrating over the free-energy difference and mutual information density.

Employing the relations discussed in Sec. II, we obtain a QDFR with feedback for the mixed work PDF [see

Eq. (B15)]

$$\frac{P_F(k, l; W)}{P_B(l, k; -W)} = e^{\beta(W - \Delta F^{(k)}) + I^{(k, l)}}, \quad (9)$$

where

$$P_B(l, k; W) = \sum_{n, m} \tilde{p}(n, l, k, m^{(k)}) \delta[W - \tilde{W}_{nkm}] \quad (10)$$

is the mixed work PDF of the backward protocol (see Fig. 3). This QDFR applies for each history  $(k, l)$  of the feedback protocol. In Eq. (10),  $\tilde{p}(n, l, k, m^{(k)}) = \tilde{p}(n|l) \tilde{p}(l|m^{(k)}) \tilde{p}(m) p(k)$ , with  $\tilde{p}(n|l) = \text{Tr}[\tilde{P}_n^{\tau_2} \tilde{U}_{\tau_2, \tilde{\tau}_1} \tilde{\mathcal{M}}_l \tilde{U}_{\tau_2, \tilde{\tau}_1}^\dagger]$  the probability that the final energy outcome is  $\tilde{E}_n^{\tau_2}$  given that the intermediate measurement outcome was  $l$ ,  $\tilde{p}(l|m^{(k)}) = \text{Tr}[\tilde{\mathcal{M}}_l \tilde{V}_{\tilde{\tau}_1, 0}^{(k)} \tilde{P}_m^{(k)0} \tilde{V}_{\tilde{\tau}_1, 0}^{(k)\dagger}]$  the probability that the intermediate measurement outcome is  $l$  given that the initial energy outcome was  $\tilde{E}_m^{(k)0}$ ,  $\tilde{p}(m) = e^{-\beta(\tilde{E}_m^{(k)0} - \tilde{F}_0^{(k)})}$  the probability of the initial energy outcome  $\tilde{E}_m^{(k)0}$ ,  $\tilde{\tau}_1 = \tau_2 - \tau_1$  the time of the intermediate measurement, and  $\tilde{W}_{nkm} = \tilde{E}_n^{\tau_2} - \tilde{E}_m^{(k)0}$  the work value. The measurement and feedback breaks a direct relational symmetry between forward and backward processes. Therefore, the backward protocol consistent with the fluctuation relations (FRs) is structurally different from the forward protocol in the presence of feedback (see Fig. 3). We also note that an analogous relation was obtained in the classical setting in Ref. [94].

First, for each value of  $k$  associated with the different feedback operations of the forward protocol, a different initial thermal state should be prepared,  $\tilde{\rho}_0^{eq, (k)} = e^{-\beta \tilde{H}_0^{(k)}} / \tilde{Z}_0^{(k)}$ , where  $\tilde{H}_0^{(k)} = \Theta H_{\tau_2}^{(k)} \Theta^\dagger$ . These initial states are sampled with the probability  $p(k)$  that the final Hamiltonian  $H_{\tau_2}^{(k)}$  occurs in the forward protocol. Second, there is no feedback control after the intermediate measurement in the backward process, and therefore no control mismatch. Third, we do not assume that the observable is time reversal [92]. The observable to be measured at  $\tilde{\tau}_1$  should be the transformed observable  $\tilde{\mathcal{M}} = \Theta \mathcal{M} \Theta^\dagger$  whose eigenprojectors are given by  $\{\tilde{\mathcal{M}}_l = \Theta \mathcal{M}_l \Theta^\dagger\}$ .

When there is no control mismatch we can still define a forward mixed joint PDF  $P_F^{\text{wcm}}(k; W, \Delta F)$  that encompasses the relevant probabilities involved (wcm stands for “without control mismatch”). We derive yet another QDFR with feedback from the mixed work PDF without mismatch  $P_F^{\text{wcm}}(k; W)$ , which applies to each history  $k$  and is given by

$$\frac{P_F^{\text{wcm}}(k; W)}{P_B^{\text{wcm}}(k; -W)} = e^{\beta(W - \Delta F^{(k)})}, \quad (11)$$

where  $P_B^{\text{wcm}}(k; -W)$  is the associated backward mixed work PDF. In APPENDIX C we discuss these PDFs in

more detail and demonstrate the validity of the QDFRs. The QDFR given by Eq. (11) could be expected since it is known that a projective measurement performed during the dynamics does not change the FRs [93].

Next we discuss the QDFR with feedback control that is valid for the process as a whole [51]. Within our formalism, we can obtain the QDFR in a different way. Integrating the discrete variables in the mixed joint PDF, Eq. (7), we obtain the joint PDF of the feedback protocol

$$P_F(W, \Delta F, I) = \sum_{m, k, l, n} p(m^{(k)}, k, l, n) \delta[W - W_{mkn}] \times \delta[\Delta F - \Delta F^{(k)}] \delta[I - I^{(k, l)}]. \quad (12)$$

We can test the consistency of this joint PDF by calculating the averages of the individual variables. Averaging the work variable we obtain the average work of the feedback protocol,  $\langle W \rangle = \sum_{k, l} p(k, l) [\mathcal{U}(\rho_{\tau_2}^{(k, l)}) - \mathcal{U}(\rho_0^{eq})]$ , which is the average, over  $p(k, l)$ , of the work of each history  $(k, l)$ . Averaging the free energy, we obtain  $\langle \Delta F \rangle = \sum_k p(k) \Delta F^{(k)}$ , which is the weighted sum of the possible values of free-energy variation. Averaging the mutual information density, we obtain  $\langle I \rangle = \sum_{k, l} p(k, l) I^{(k, l)}$ , which is the mutual information. From Eq. (12) and the relation between forward and backward processes given in Sec. II we obtain the QDFR with feedback for the whole process [51]

$$\frac{P_F(W, \Delta F, I)}{P_B(-W, -\Delta F, I)} = e^{\beta(W - \Delta F) + I}, \quad (13)$$

where

$$P_B(W, \Delta F, I) = \sum_{n, l, k, m} \tilde{p}(n, l, k, m^{(k)}) \delta[W - \tilde{W}_{nkm}] \times \delta[\Delta F - \Delta \tilde{F}^{(k)}] \delta[I - I^{(k, l)}] \quad (14)$$

is the associated joint PDF of the backward protocol (see also APPENDIX D).

The characteristic function of a PDF is given by its Fourier transform and contains as much information as the PDF itself. Our method to experimentally verify the QDFR with feedback control relies on the direct measurement of the characteristic functions associated with the PDFs appearing in the FRs discussed above. Without the presence of feedback control, a method to obtain the characteristic functions of work distributions was introduced in Refs. [62, 63] and successfully applied in an experimental scenario in Refs. [26, 27]. Here we extend these ideas for discrete feedback-controlled quantum processes and, as will be seen, the complexity of the method increases considerably. We write down explicitly these characteristic functions below (see APPENDIX E). From the forward and backward mixed work PDFs, Eqs. (8) and (10), we obtain

$$\chi_F^{(k,l)}(u) = p(k|l) \text{Tr} \left[ e^{+iuH_{\tau_2}^{(k)}} V_{\tau_2, \tau_1}^{(k)} \mathcal{M}_l U_{\tau_1, 0} e^{-iuH_0} \rho_0^{eq} U_{\tau_1, 0}^\dagger \mathcal{M}_l V_{\tau_2, \tau_1}^{(k)\dagger} \right], \quad (15)$$

$$\chi_B^{(l,k)}(u) = p(k) \text{Tr} \left[ e^{+iu\tilde{H}_{\tau_2}} \tilde{U}_{\tau_2, \tilde{\tau}_1} \tilde{\mathcal{M}}_l \tilde{V}_{\tilde{\tau}_1, 0}^{(k)} e^{-iu\tilde{H}_0} \tilde{\rho}_0^{eq, (k)} \tilde{V}_{\tilde{\tau}_1, 0}^{(k)\dagger} \tilde{\mathcal{M}}_l \tilde{U}_{\tau_2, \tilde{\tau}_1}^\dagger \right], \quad (16)$$

where we take the Fourier transformation of the work variable  $W$  and  $u$  is the transformed variable associated with the quantum work. For further reference throughout this paper, we denote the trace in Eq. (16) by  $\mathcal{A}(k, l) = \chi_B^{(l,k)}(u) / p(k)$ .

From the forward and backward joint PDFs, Eqs. (12) and (14), we obtain

$$\chi_F(u, v, w) = \sum_{k,l} e^{iuvI^{(k,l)}} e^{iv\Delta F^{(k)}} \chi_F^{(k,l)}(u), \quad (17)$$

$$\chi_B(u, v, w) = \sum_{l,k} e^{iuvI^{(k,l)}} e^{iv\Delta \tilde{F}^{(k)}} \chi_B^{(k,l)}(u), \quad (18)$$

where  $u$ ,  $v$ , and  $w$  are the transformed variables associated with the stochastic work  $W$ , free-energy variation  $\Delta F^{(k)}$ , and mutual information density  $I^{(k,l)}$ , respectively.

#### IV. VERIFYING QUANTUM DETAILED FLUCTUATION RELATIONS IN THE PRESENCE OF FEEDBACK CONTROL

In this section we present a feasible method to experimentally verify the QDFR for feedback processes, Eq. (13). The method is schematically depicted in Fig. 4 and the strategy is as follows. In order to experimentally obtain the forward and backward joint PDFs, Eqs. (12) and (14), we will describe a way to measure the corresponding characteristic functions, Eqs. (17) and (18). The joint PDFs can be obtained from the inverse Fourier transform of the associated characteristic functions.

For the full reconstruction of the PDFs in the presence of feedback, four quantities are required. The characteristic functions of the forward and backward mixed PDFs, Eqs. (15) and (16), are directly obtained from the interferometric quantum algorithms that we will introduce in what follows. The remaining two quantities are the free-energy differences and the mutual information density. Using the relation between forward and backward processes, it can be shown that  $\Delta \tilde{F}^{(k)} = -\Delta F^{(k)}$  and therefore only the forward free-energy differences are really needed.

The forward free-energy differences can be obtained from the QDFR without control mismatch, Eq. (11), using an adaptation of the methods developed in Refs. [26, 27] and which we will detail below. The characteristic functions of the forward and backward mixed work PDF without control mismatch,  $P_F^{\text{wcm}}(k; W)$  and  $P_B^{\text{wcm}}(k; W)$ , which we denote as  $\chi_F^{\text{wcm}(k)}(u)$  and  $\chi_B^{\text{wcm}(k)}(u)$ , respectively, will also be required (see also APPENDIX E).

The mutual information density can be analogously obtained from the QDFR with control mismatch, Eq. (9), which involves the characteristic functions  $\chi_F^{(k,l)}(u)$  and  $\chi_B^{(l,k)}(u)$ . In summary, it is necessary to experimentally measure four characteristic functions. Our method proposes five quantum algorithms which accomplish this task using an interferometric strategy and auxiliary quantum systems that will encode the characteristic function to be measured.

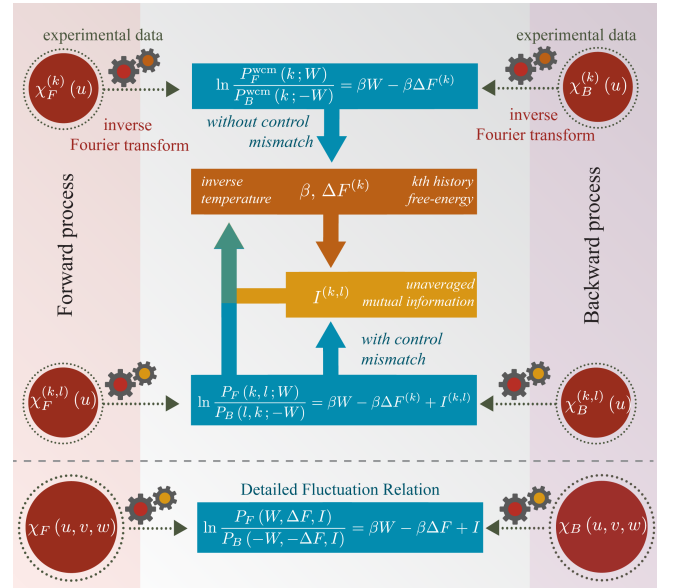


Figure 4. Flowchart representing the proposed method to verify the QDFR in the presence of feedback control (in blue below the dashed line). The four characteristic functions represented above the dashed line are the experimental data needed for the verification. They are obtained from measurements of five quantum algorithms. Taking their inverse Fourier transform we use the corresponding PDFs in the two QDFRs displayed in blue. The QDFR without control mismatch (uppermost) is used to obtain the free energy differences  $\Delta F^{(k)}$ . The QDFR with control mismatch (just above the dashed line) and the free energies previously obtained are used to obtain the mutual information density  $I^{(k,l)}$ . If wanted, several independent estimations of the initial inverse temperature  $\beta$  can be obtained as explained in the text. With the free-energy differences, the mutual information density and the forward,  $\chi_F^{(k,l)}(u)$ , and backward,  $\chi_B^{(l,k)}(u)$ , characteristic work functions, the joint forward and backward characteristic functions (below the dashed line) can be reconstructed. By inverse Fourier transform the QDFR for discrete feedback processes can be verified through multiple linear regression (see Fig. F1 in APPENDIX F for an additional description of the method).

Here we employ a full quantum perspective for the feedback protocol illustrated in Fig. 2, which is expressed by the fact that feedback controller is regarded as a quantum system. The characteristic function of the forward mixed work PDF,  $\chi_F^{(k,l)}(u)$ , has two fixed parameters,  $k$  and  $l$ . Our algorithm employs two quantum memories to store the information concerning these parameters. These memories should have a state space dimension at least as large as the ranges of the indices  $k$  and  $l$  so as to encode them in orthogonal states. Moreover, an ancilla qubit is used to encode the information of the characteristic function [62]. We assume from now on, without loss of generality, that the system of interest is a qubit. Hence, the two memories, which we designate as the feedback controller memories, are two qubits. We stress that the ancilla system (which encodes the characteristic function) can always be a qubit, irrespective of the dimension of the system of interest. Notwithstanding, the ideas presented here can be extended to other scenarios: where the control has a fixed probability to fail or to a semiclassical feedback device where the feedback memory and control mechanism are classical objects.

The quantum interferometric circuit depicted in Fig. 5 enables the measurement of the characteristic function  $\chi_F^{(k,l)}(u)$ . The measurement stage of the feedback is implemented by an emulated nonselective measurement. This is accomplished by an  $\mathcal{M}$ -CNOT gate (right after the unitary gate  $U_{\tau_1,0}$  in Fig. 5). This gate is similar to the usual CNOT gate, except that the control basis is not the computational basis,  $\{|0\rangle, |1\rangle\}$ , but the basis of the eigenvectors of the observable  $\mathcal{M}$  to be measured in the feedback protocol [see Eq. (F1)]. We consider one extra rotation ( $\mathcal{R}_\varphi = e^{-i\varphi\sigma_x}$  in Fig. 5) that plays the role of switching the control mismatch in the feedback protocol.

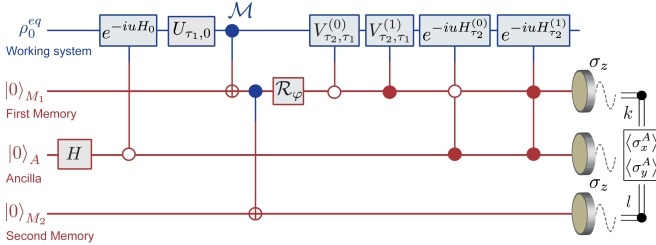


Figure 5. Quantum interferometric circuit for the measurement of the forward work characteristic function with control mismatch,  $\chi_F^{(k,l)}(u)$ . The nonselective measurement is implemented with a  $\mathcal{M}$ -CNOT gate. The rotation  $\mathcal{R}_\varphi$  changes the memory states so that the feedback is implemented with control mismatch. After a measurement in the computational basis of the two memories (of the feedback protocol),  $M_1$  and  $M_2$ , whose outcomes  $(k, l)$  occur with probability  $p^{M_1 M_2}(k, l)$ , the ancilla  $A$  encodes the characteristic function in its coherence elements in the computational basis. It can be retrieved from the average of the Pauli observables in the auxiliary system  $\langle \sigma_x^A \rangle = \text{Re} [\chi_F^{(k,l)}(u)] / p^{M_1 M_2}(k, l)$  and  $\langle \sigma_y^A \rangle = \text{Im} [\chi_F^{(k,l)}(u)] / p^{M_1 M_2}(k, l)$ .

The feedback stage is implemented, in a quantum way, by controlled unitary gates to properly perform the correct feedback operations  $V_{\tau_2, \tau_1}^{(k)}$  using the encoded information in the quantum memory.

When the feedback device is described as a quantum system, which is our case here, the state of the composite system at the end of the interferometric circuit may be highly entangled. At the end of the circuit a measurement in the computational basis of the two memory qubits is performed giving outcomes  $(k, l)$  with probability  $p^{M_1 M_2}(k, l)$  [for details see Eq. (G1)]. After such a measurement, the ancillary qubit  $A$  encodes the information of the forward work characteristic function associated with the corresponding outcome and feedback control operation  $(k, l)$ ,  $\chi_F^{(k,l)}(u)$ .

The characteristic function and its conjugate are encoded in the coherence elements of the reduced density matrix of the ancilla in the computational basis. It can be extracted from the averages  $\langle \sigma_x^A \rangle = \text{Re} [\chi_F^{(k,l)}(u)] / p^{M_1 M_2}(k, l)$  and  $\langle \sigma_y^A \rangle = \text{Im} [\chi_F^{(k,l)}(u)] / p^{M_1 M_2}(k, l)$  of the Pauli observables  $\sigma_x^A$  and  $\sigma_y^A$  in the ancillary qubit  $A$ .

In the actual implementation of the interferometric circuit, the conjugate variable  $u$  will be associated with the time of a suitable interaction between the qubits implementing the controlled unitaries. Therefore, each run of the algorithm actually measures a single value of the characteristic function, i.e., for a given interaction time and thus a given value of  $u$ . This means that the quantum algorithm has to run several times to obtain a discretized characteristic function [26]. The sampling rate of the parametrization of  $u$ , in an actual experiment, will be also related to the accuracy of the inverse Fourier transform of the acquired data in order to reconstruct the work PDFs.

When there is no feedback control mismatch, one memory to encode the value of  $k$  suffices. The quantum circuit which measures the characteristic work function  $\chi_F^{\text{wcm}(k)}(u)$  is shown in Fig. 6. As before,  $\chi_F^{\text{wcm}(k)}(u)$  is encoded in the coherence elements of the ancilla in the computational basis when the (feedback) memory measurement outcome  $k$  is obtained. This occurs with probability  $p^M(k)$  [see also Eq. (G2)]. In this case, the average of the Pauli observables  $\langle \sigma_x^A \rangle = \text{Re} [\chi_F^{\text{wcm}(k)}(u)] / p^M(k)$  and  $\langle \sigma_y^A \rangle = \text{Im} [\chi_F^{\text{wcm}(k)}(u)] / p^M(k)$  provides the real and imaginary parts of the characteristic function.

To measure the backward characteristic function  $\chi_B^{\text{wcm}(k)}(u)$  without control mismatch the quantum algorithm in Fig. 7 will be employed. The strategy of the interferometric protocol is as follows. Prepare the thermal initial state of the backward protocol,  $\tilde{\rho}_0^{eq,(k)} = e^{-\beta \tilde{H}_0} / \tilde{Z}_0^{(k)}$ . When the measurement outcome of the feedback memory measurement is  $l \neq k$ , the data are discarded and the initial state is prepared again. When the measurement outcome of the feed-



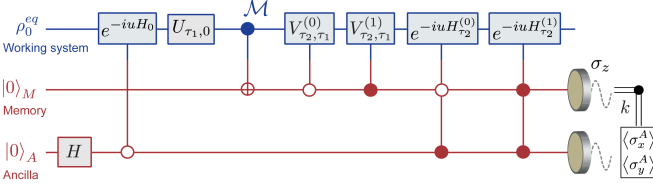


Figure 6. Quantum interferometric circuit for the measurement of the forward characteristic work function without control mismatch  $\chi_F^{(k)}(u)$ . After a measurement in the computational basis of the memory  $M$  [whose outcomes  $k$  occur with probability  $p^M(k)$ ], the ancilla  $A$  encodes the characteristic function in its coherence elements in the computational basis. It can be retrieved from the average of the Pauli observables  $\langle \sigma_x^A \rangle = \text{Re}[\chi_F^{(k)}(u)]/p^M(k)$  and  $\langle \sigma_y^A \rangle = \text{Im}[\chi_F^{(k)}(u)]/p^M(k)$ .

back memory is  $l = k$ , the ancilla  $A$  encodes the information of  $\chi_B^{\text{wcm}(k)}(u)$  in its coherences in the computational basis. Again, the average of the Pauli observables  $\langle \sigma_x^A \rangle = \text{Re}[\chi_B^{\text{wcm}(k)}(u)]/p_B^M(l = k)$  and  $\langle \sigma_y^A \rangle = \text{Im}[\chi_B^{\text{wcm}(k)}(u)]/p_B^M(l = k)$  is used to construct the characteristic function. The probability  $p_B^M(l)$  is the probability that the memory measurement provides the outcome  $l$  [see Eq. (G3)].

The backward characteristic work function with mismatch,  $\chi_B^{(l,k)}(u)$ , requires two quantum circuits: the one we just considered in Fig. 7 and the one depicted in Fig. 8. This latter circuit measures the joint probability  $p(k, l)$  from the statistics of the composite measurement  $\mathcal{M}^S \otimes \sigma_z^M$ . This is necessary to obtain the distribution  $p(k) = \sum_{k,l} p(k, l)$  that appears in Eq. (16). The trace in Eq. (16), denoted by  $\mathcal{A}(k, l)$ , is obtained by the measurement of the ancilla qubit in Fig. 7. The average of the Pauli observables  $\langle \sigma_x^A \rangle = \text{Re}[\mathcal{A}(k, l)]/p_B^M(l)$  and  $\langle \sigma_y^A \rangle = \text{Im}[\mathcal{A}(k, l)]/p_B^M(l)$  enables the reconstruction of  $\mathcal{A}(k, l)$  (see APPENDIX F). With  $p(k)$  and  $\mathcal{A}(k, l)$  one can reconstruct  $\chi_B^{(l,k)}(u) = p(k) \mathcal{A}(k, l)$  [see Eq. (16)].

We have hitherto shown how to obtain the four characteristic work functions:  $\chi_F^{\text{wcm}(k)}(u)$  for the forward process without mismatch,  $\chi_B^{\text{wcm}(k)}(u)$  for the backward process without mismatch,  $\chi_F^{(k,l)}(u)$  for the forward process with mismatch, and  $\chi_B^{(l,k)}(u)$  for the backward process with mismatch. Thus, by means of the inverse Fourier transform, one can obtain the four corresponding mixed work PDFs:  $P_F^{\text{wcm}}(k; W)$  for the forward process without mismatch,  $P_B^{\text{wcm}}(k; W)$  for the backward process without mismatch,  $P_F(k, l; W)$  for the forward process with mismatch, and  $P_B(l, k; W)$  for the backward process with mismatch.

For the moment, let us consider the mixed work PDFs without mismatch,  $P_F^{\text{wcm}}(k; W)$  and  $P_B^{\text{wcm}}(k; W)$ . For a system with discrete energy spectrum these PDFs should be theoretically given by a sum of delta functions with all

the possible transitions from the eigenstates of the initial Hamiltonian to the eigenstates of the final Hamiltonian. For a feedback-driven qubit dynamics in which the initial and final Hamiltonians have different energy spectra, each of these PDFs has four different peaks for each  $k$  [26]. The peaks of the forward and backward PDFs will coincide because  $E_m^{(k)\tau_2} - E_n^0 = -(\tilde{E}_n^{\tau_2} - \tilde{E}_m^{(k)0})$  from the relations discussed in Sec. II. The peaks will differ only by multiplicative factors, i.e., the factors multiplying the delta functions [see Eqs. (20) and (22) of the next section].

Taking the ratio of the two PDFs and then the logarithm, one obtains  $\ln P_F^{\text{wcm}}(k; W)/P_B^{\text{wcm}}(k; W) = \beta W - \beta \Delta F^{(k)}$ , which is the QDFR without mismatch, Eq. (11). For each  $k$ , a logarithmic plot of this ratio will provide a set of points which ideally lie in a straight line. From each straight line, one can infer the inverse temperature  $\beta$  from the slope and the free-energy difference  $\Delta F^{(k)}$  for each history from the interception of the line with the vertical axis.

The same reasoning applies to the forward,  $P_F(k, l; W)$ , and backward,  $P_B(l, k; W)$ , PDFs with control mismatch. In that case, the logarithm of the ratio is  $\ln P_F(k, l; W)/P_B(l, k; W) = \beta W - \beta \Delta F^{(k)} + I^{(k,l)}$ , which is the QDFR with mismatch, Eq. (9). For each history  $(k, l)$  the logarithmic plot of the ratio will provide a set of points which ideally lie in a straight

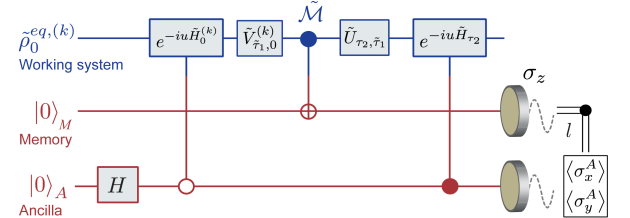


Figure 7. Quantum interferometric circuit for the measurement of the backward characteristic work functions with and without mismatch,  $\chi_B^{(l,k)}(u)$  and  $\chi_B^{\text{wcm}(k)}(u)$ , respectively. In order to measure  $\chi_B^{\text{wcm}(k)}(u)$  the ancilla  $A$  is measured only when the outcome of the memory measurement  $M$  is  $l = k$ . After a measurement of the feedback memory in the computational basis, whose outcomes  $l$  occur with probability  $p_B^M(l)$ , the ancilla encodes the information of  $\mathcal{A}(k, l)$  [defined after Eq. (16)] in its coherence elements in the computational basis. The information can be retrieved from the average of the Pauli observables  $\langle \sigma_x^A \rangle = \text{Re}[\mathcal{A}(k, l)]/p_B^M(l)$  and  $\langle \sigma_y^A \rangle = \text{Im}[\mathcal{A}(k, l)]/p_B^M(l)$ . For the case where feedback occurs without control mismatch the equality  $\chi_B^{\text{wcm}(k)}(u) = \mathcal{A}(k, k)$  holds. Therefore, in that case, the ancilla encodes the characteristic function as  $\langle \sigma_x^A \rangle = \text{Re}[\chi_B^{\text{wcm}(k)}(u)]/p_B^M(l = k)$  and  $\langle \sigma_y^A \rangle = \text{Im}[\chi_B^{\text{wcm}(k)}(u)]/p_B^M(l = k)$ . With control mismatch the equality  $\chi_B^{(l,k)}(u) = p(k) \mathcal{A}(k, l)$  holds. Therefore, the average of the ancilla Pauli observables provides part of the backward characteristic function. The probability  $p(k)$  is measured with the quantum circuit in Fig. 8.

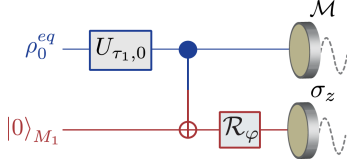


Figure 8. Quantum circuit to characterizing the feedback mechanism. It may be employed for the determination of the joint probability distribution  $p(k, l)$  of the  $(k, l)$  history. A composite measurement of the joint observable  $\mathcal{M}^S \otimes \sigma_z^M$  gives outcomes  $(k, l)$  with probability  $p(k, l)$ .

line. From each straight line one can independently obtain the inverse temperature  $\beta$  from the slopes. The points of interception with the vertical axis give the quantities  $I^{(k,l)} - \beta \Delta F^{(k)}$ . Since  $\beta$  was determined from the corresponding slope and  $\Delta F^{(k)}$  from the QDFR without control mismatch, one can infer the values of the mutual information density  $I^{(k,l)}$  from the interception points. The nonidealities inevitably associated with actual experiments are discussed in the next section when we consider a concrete example.

From our discussion at the beginning of this section, we explained how to obtain (via an interferometric strategy) the four quantities required to reconstruct the joint forward and backward characteristic functions,  $\chi_F(u, w, v)$  and  $\chi_B(u, w, v)$ . One can infer the free energies  $\Delta F^{(k)}$  and the mutual information density  $I^{(k,l)}$  and directly measure  $\chi_F^{(k,l)}(u)$  and  $\chi_B^{(l,k)}(u)$  from the quantum circuits as explained. The forward,  $P_F(W, \Delta F, I)$ , and backward,  $P_B(W, \Delta F, I)$ , joint PDFs can be obtained from the inverse Fourier transform of the corresponding characteristic functions.

The logarithm of the ratio of the two PDFs  $\ln P_F(W, \Delta F, I) / P_B(W, \Delta F, I) = \beta W - \beta \Delta F + I$ , which is the logarithm of the QDFR introduced in Eq. (13). As these PDFs depend on three stochastic variables  $W$ ,  $\Delta F$ , and  $I$ , the logarithmic plot of their ratio will be related to a set of points in four dimensions. Moreover, denoting by  $z = f(W, \Delta F, I)$  the logarithm of the ratio, these points should ideally lie in a hyperplane given by the equation  $\beta W - \beta \Delta F + I - z = 0$ . The parameters  $\beta$ ,  $-\beta$ , and 1 that multiply the variables  $W$ ,  $\Delta F$ , and  $I$ , respectively, can be obtained using multiple linear regression.

Further details are discussed in the illustrative example provided in the next section. We note that the coefficient of the mutual information density  $I$  is independent of any parameter of the protocols. Consequently, the analysis of how much this coefficient differs from 1 using the experimental data is a robust consistency test of the QDFR for feedback control protocols.

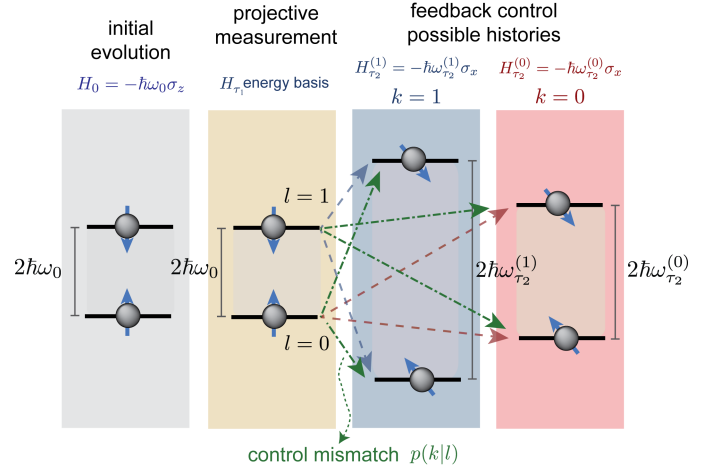


Figure 9. Representation of the feedback control protocol considered in the illustrative example. The system starts in the thermal state with Hamiltonian  $H_0 = -\hbar\omega_0\sigma_z$  and inverse temperature  $\beta$ . The Hamiltonian is kept constant up to time  $\tau_1$  along a free evolution,  $H_{\tau_1} = H_0$ . At time  $\tau_1$ , the feedback measurement is performed. We considered the instantaneous Hamiltonian as the measurement observable. The feedback operation corresponding to  $k = 0$  ( $k = 1$ ) is a sudden change of the Hamiltonian from  $H_0$  to  $H_{\tau_1}^{(0)} = -\hbar\omega_{\tau_2}^{(0)}\sigma_x$  ( $H_{\tau_1}^{(1)} = -\hbar\omega_{\tau_2}^{(1)}\sigma_x$ ). Whichever the case, the Hamiltonian is kept constant up to time  $\tau_2$ . If there is no control mismatch, the red (blue) arrows correspond to the possible transitions among the instantaneous eigenstates in the TPM scheme corresponding to  $l = k = 0$  ( $l = k = 1$ ). The control mismatch will be modeled by an  $x$ -rotation on the feedback memory changing the reference basis for the feedback implementation from the computational basis. The control mismatch probability is parametrized by a single angle  $\varphi$  through  $p(k|l) = \langle k | R_x(\varphi) | l \rangle$  and the transitions are depicted by the green arrows.

## V. ILLUSTRATIVE EXAMPLE: QUBIT CONTROLLED BY CONDITIONAL QUENCHES

Let us consider a qubit which is controlled by a conditional sudden quench, in a similar way to what was experimentally implemented in a spin-1/2 system in Ref. [59]. After the measurement stage of the feedback protocol, the system is driven in two different ways, depending on the measurement outcome. Elements of the protocol are outlined in Fig. 9. The qubit starts in the Gibbs state with initial Hamiltonian  $H_0 = -\hbar\omega_0\sigma_z$ . In the pre-measurement part of the protocol, the Hamiltonian remains constant up to time  $\tau_1$ , hence the evolution operator is given by  $U_{\tau_1,0} = \exp\{+i\omega_0\tau_1\sigma_z\}$  and the population of the systems state does not change. The associated work of this process is zero since there is no external drive. Then, a measurement of the Hamiltonian  $H_{\tau_1} = H_0$  is performed at time  $\tau_1$ . The measurement projectors are denoted by  $\mathcal{M}_l = |l\rangle\langle l|$ , where  $|0\rangle$  and  $|1\rangle$  are the eigenstates of  $\sigma_z$  with positive and negative eigenvalues, respectively.

The feedback control mismatch is modeled by a single parameter  $\varphi$ , i.e.,  $p(k|l) = \langle k | R_x(\varphi) | l \rangle$ , where  $R_x(\varphi) = \exp\{-i\varphi\sigma_x\}$  is an  $x$  rotation. When  $\varphi = 0$  there is no mismatch between the measurement basis and the reference basis which applies the feedback operations. When the mismatch angle is different from zero, the measurement basis (computational basis) will be different from the basis which implements the feedback. In the latter case the reference basis for the feedback is the basis obtained by performing the  $x$  rotation with an angle  $\varphi$  onto the computational basis.

The index  $k$  represents the feedback operation being performed on the postmeasurement state whereas  $l$  is the actual measurement outcome. Without control mismatch we would have  $k = l$ . If  $k = 0$ , the Hamiltonian is suddenly changed to  $H_{\tau_1}^{(0)} = -\hbar\omega_{\tau_2}^{(0)}\sigma_x$  and then kept constant up to time  $\tau_2$ . Hence, the evolution operator is  $V_{\tau_2, \tau_1}^{(0)} = \exp\left\{+i\omega_{\tau_2}^{(0)}(\tau_2 - \tau_1)\sigma_x\right\}$  and the final Hamiltonian is  $H_{\tau_2}^{(0)} = H_{\tau_1}^{(0)}$ . If  $k = 1$ , the Hamiltonian is suddenly changed to  $H_{\tau_1}^{(1)} = -\hbar\omega_{\tau_2}^{(1)}\sigma_x$  and then kept constant up to time  $\tau_2$ . Hence, the evolution operator is  $V_{\tau_2, \tau_1}^{(1)} = \exp\left\{+i\omega_{\tau_2}^{(1)}(\tau_2 - \tau_1)\sigma_x\right\}$  and the final Hamiltonian is  $H_{\tau_2}^{(1)} = H_{\tau_1}^{(0)}$ . The difference between the two feedback operations is the energy gap between the qubit eigenstates ( $\hbar\omega_{\tau_2}^{(0)}$  and  $\hbar\omega_{\tau_2}^{(1)}$ ). For a spin-1/2 particle these sudden changes correspond to fast switches in the magnetic-field direction and intensity. Furthermore, for the sake of illustration, we assume that  $\omega_{\tau_2}^{(0)} = 2\omega_0$ ,  $\omega_{\tau_2}^{(1)} = 3\omega_0$ , and  $5\hbar\omega_0 = k_B T$ .

With the protocol properly defined, the quantum algorithms introduced in the preceding section have to be performed in order to obtain the quantities of interest. In the case in which there is no mismatch, the characteristic work function for a single history is obtained by performing the algorithm in Fig. 6. In other words, the characteristic function will be encoded in the auxiliary system  $A$ , and reads

$$\chi_F^{\text{wcm}(k)}(u) = \frac{1}{2} \frac{e^{-\beta E_k^0}}{Z_0} \left[ e^{iu(E_1^{(k, \tau_2)} - E_k^0)} + e^{iu(E_0^{(k, \tau_2)} - E_k^0)} \right]. \quad (19)$$

This characteristic function leads to the mixed work PDF

$$P_F^{\text{wcm}}(k; W) = \frac{1}{2} \frac{e^{-\beta E_k^0}}{Z_0} \left[ \delta \left[ W - \left( E_1^{(k, \tau_2)} - E_k^0 \right) \right] + \delta \left[ W - \left( E_0^{(k, \tau_2)} - E_k^0 \right) \right] \right]. \quad (20)$$

In actual experimental realizations, the oscillatory complex functions in Eq. (19) may be restricted to some time interval and the values of the variable  $u$  are discrete with some suitable sampling rate [26]. This, in turn, will lead to a set of finite width distributions for the PDFs (actual experimental data), in this case Lorentz distributions, instead of delta functions (as in the idealized theory). In

what follows, we plot representative values for the quantities with mismatch.

The backward process will be defined by the corresponding time-reversal operator for a spin-1/2 particle [85],  $\Theta = i\sigma_y K$ , where  $K[\cdot]$  is the conjugation map. Therefore,  $\tilde{H}(t) = i\sigma_y K[H(t) iK[\sigma_y]] = \sigma_y H(t)^* \sigma_y$ , where  $H(t)$  is assumed to be written in the computation basis and we used  $\Theta^\dagger = iK[\sigma_y] = -i\sigma_y$ . Observe that  $K[\cdot]$  has to be interpreted as a map applied to everything after it. The backward Hamiltonians turn out to be  $\tilde{H}_0^{(0)} = \hbar\omega_{\tau_2}^{(0)}\sigma_x$ ,  $\tilde{H}_0^{(1)} = \hbar\omega_{\tau_2}^{(1)}\sigma_x$ , and  $\tilde{H}_{\tau_2} = \hbar\omega_0\sigma_z$ .

Let us emphasize an important detail discussed at the end of Sec. III A. Consider the qubit system is encoded in a spin-1/2 particle immersed in an external magnetic field. A change in the magnetic-field direction would change the sign of the Larmor frequency  $\omega$ . Therefore, one could interpret the minus sign difference between the forward  $H$  and backward  $\tilde{H}$  Hamiltonians to be a change in the direction of the magnetic field. However, the time-reversal transformation changes the sign of the spin operator, a property of the system, and not the sign of the magnetic field, which is a property of the environment where the system is immersed (the control system). Therefore, we conclude that the time-reversal transformation has the same dynamical effect on the spin as would be a change in the external magnetic-field direction. Thus, in the actual experiment, the backward Hamiltonian can be implemented by the reversal of the magnetic-field direction and its time modulation. We emphasize that this is possible due to the dynamical equivalence of the time-reversed Hamiltonian and the Hamiltonian with magnetic-field direction reversed. This dynamical equivalence was exploited in Refs. [26, 27] to experimentally implement the backward protocol.

The evolution operators of the two possible backward process are  $\tilde{V}_{\tau_1, 0}^{(0)} = \exp\left\{-i\omega_{\tau_2}^{(0)}\tilde{\tau}_1\sigma_x\right\}$ ,  $\tilde{V}_{\tau_1, 0}^{(1)} = \exp\left\{-i\omega_{\tau_2}^{(1)}\tilde{\tau}_1\sigma_x\right\}$ , and  $\tilde{U}_{\tau_2, \tau_1} = \exp\left\{-i\omega_0\tau_1\sigma_z\right\}$ , where  $\tilde{\tau}_1 = \tau_2 - \tau_1$ . To obtain the backward characteristic work function without control mismatch the quantum algorithm in Fig. 7 has to be implemented. In the preceding section we discussed that, in the absence of control mismatch, one has to consider only the situations when  $l = k$ . This means that if the Gibbs state  $\tilde{\rho}_0^{eq, (0)}$ , associated with the time-reversed initial Hamiltonian  $\tilde{H}_0^{(0)}$ , is prepared, then only the values obtained for the ancilla observables corresponding to the outcome of the memory measurement  $l = k = 0$  has to be considered. Conversely, when the initial state is the Gibbs state  $\tilde{\rho}_0^{eq, (1)}$ , associated with the Hamiltonian  $\tilde{H}_0^{(1)}$ , the statistics of the measurements on the ancilla when the memory measurement outcome is  $l = k = 1$  have to be considered. In summary, an outcome-dependent postprocessing of the data has to be done. This will provide the characteristic

function

$$\chi_B^{\text{wcm}(k)}(u) = \frac{1}{2} \frac{e^{-\beta \tilde{E}_0^{(k)0}}}{\tilde{Z}_0^{(k)}} e^{iu(\tilde{E}_k^{\tau_2} - \tilde{E}_0^{(k)0})} + \frac{1}{2} \frac{e^{-\beta \tilde{E}_1^{(k)0}}}{\tilde{Z}_0^{(k)}} e^{iu(\tilde{E}_k^{\tau_2} - \tilde{E}_1^{(k)0})}. \quad (21)$$

This characteristic function leads to the mixed work PDF

$$P_B^{\text{wcm}}(k; W) = \frac{1}{2} \frac{e^{-\beta \tilde{E}_0^{(k)0}}}{\tilde{Z}_0^{(k)}} \delta \left[ W - (\tilde{E}_k^{\tau_2} - \tilde{E}_0^{(k)0}) \right] + \frac{1}{2} \frac{e^{-\beta \tilde{E}_1^{(k)0}}}{\tilde{Z}_0^{(k)}} \delta \left[ W - (\tilde{E}_k^{\tau_2} - \tilde{E}_1^{(k)0}) \right]. \quad (22)$$

The next step is to take the ratio of the forward [Eq. (20)] and backward [Eq. (22)] PDFs. In our theoretical example this is simply done by taking the ratio of the coefficients preceding the corresponding delta functions. However, the actual data would consist, typically, of a sum of Lorentz distributions which possess finite width. Therefore, an estimator for the best representative value of the heights would have to be considered. For instance, an estimator would simply consider Lorentz distributions that fit the experimental data.

In our example, the PDFs have two terms, so the ratio of the PDFs provides two points for each value of  $k$ . In Fig. 10 we show the result of this ratio plotted on a logarithmic scale. From the QDFR without mismatch for each  $k$ , the straight lines connecting the corresponding pair of points should be equal to

$$\ln \frac{P_F^{\text{wcm}}(k; W)}{P_B^{\text{wcm}}(k; -W)} = \beta W - \beta \Delta F^{(k)}. \quad (23)$$

The interception of the graph with the vertical axis should approximately be  $-\beta \Delta F^{(k)}$ . Therefore, the free-energy variation can be estimated, given that  $\beta$  was obtained from the slope of the best line fitting the data. However, the value of  $\beta$  may contain experimental errors which also propagate to this estimation of the free energies  $\Delta F^{(k)}$ . A better strategy to estimate the free energies is the following. When the vertical axis is equal to one, the left-hand side of Eq. (23) implies that  $W = \Delta F^{(k)}$  (since we are using a logarithmic scale). Therefore, for each  $k$ , the corresponding value of  $W$  when the image is 1 provides an estimation of the corresponding free-energy difference  $\Delta F^{(k)}$ . Such estimation would encompass the experimental errors of the linear fit avoiding the error propagation from the inverse temperature in the direct determination of the linear coefficient,  $-\beta \Delta F^{(k)}$ , of the fitting curve.

Let us consider now the case with control mismatch. The forward characteristic work function is obtained from the quantum algorithm in Fig. 5. For our example this will give

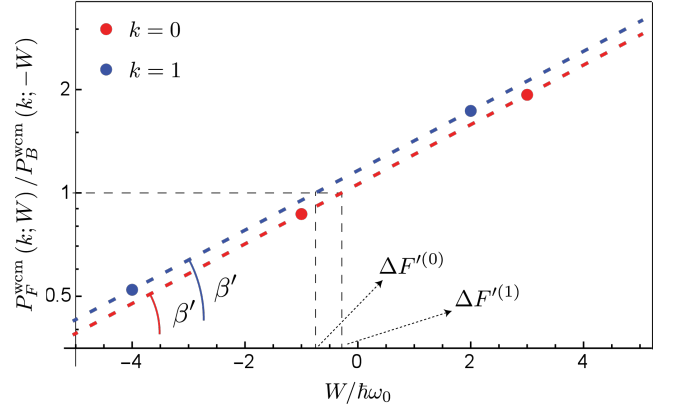


Figure 10. Logarithmic plot of the QDFR for a single history without mismatch. The four points show the possible transitions which may occur in the forward process if the outcome of the measurement is  $k = 0$  (red) or  $k = 1$  (blue). The straight dashed lines represent the linear fit which should be related to the two functions  $\beta W^{(k)} - \beta \Delta F^{(k)}$ , for both outcomes,  $k = 0$  (red) or  $k = 1$  (blue). From each curve, one can obtain  $\beta$  from the slope and  $\Delta F^{(k)}$  from the work value whose image is 1. Since in our analytical example we plotted the normalized work variable  $W/\hbar\omega_0$ , the slope actually provides  $\beta' = \hbar\omega_0\beta$  and the values whose image is 1 are  $\Delta F'^{(k)} = \Delta F^{(k)}/\hbar\omega_0$ . We assumed that  $\omega_{\tau_2}^{(0)} = 2\omega_0$ ,  $\omega_{\tau_2}^{(1)} = 3\omega_0$ , and  $5\hbar\omega_0 = k_B T$ .

$$\chi_F^{(k,l)}(u) = \frac{1}{2} p(k|l) \frac{e^{-\beta E_l^0}}{Z_0} [e^{iu(E_1^{(k,\tau_2)} - E_l^0)} + e^{iu(E_0^{(k,\tau_2)} - E_l^0)}]. \quad (24)$$

In Fig. 11 we show its real part when the mismatch angle is  $\varphi = \pi/3$ . The corresponding mixed work PDF is obtained by the inverse Fourier transform of the measured forward characteristic work function and should be

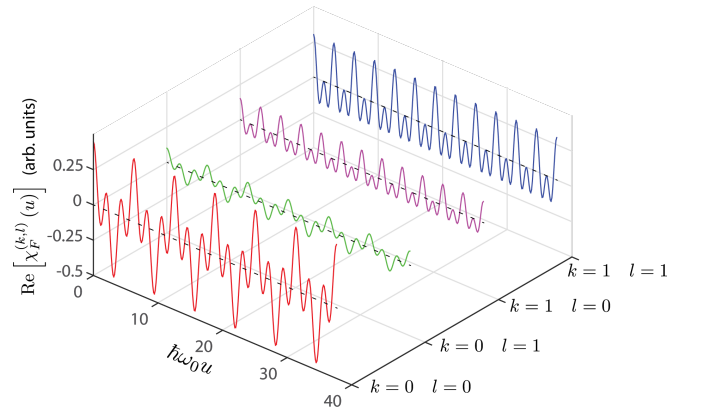


Figure 11. Real part of the forward work characteristic function with control mismatch,  $\chi_F^{(k,l)}(u)$ , for each history  $(k, l)$ . We assumed that  $\omega_{\tau_2}^{(0)} = 2\omega_0$ ,  $\omega_{\tau_2}^{(1)} = 3\omega_0$ ,  $5\hbar\omega_0 = k_B T$ , and  $\varphi = \pi/3$ .



related to

$$P_F(k, l; W) = \frac{1}{2} p(k|l) \frac{e^{-\beta E_l^0}}{Z_0} [\delta[W - (E_1^{(k, \tau_2)} - E_l^0)] + \delta[W - (E_0^{(k, \tau_2)} - E_l^0)]] \quad (25)$$

In Fig. 12 we plot the four mixed work PDFs when  $\varphi = \pi/3$ .

Recall that we need two quantum algorithms to obtain the backward characteristic work function with mismatch,  $\chi_B^{(l, k)}(u)$ . The probability  $p(k)$  is obtained from the circuit displayed in Fig. 8, while the trace  $\mathcal{A}(k, l)$  in  $\chi_B^{(l, k)}(u)$  [introduced in Eq. (16)] is obtained from the circuit in Fig. 7. Together they will give

$$\chi_B^{(l, k)}(u) = \frac{1}{2} p(k) \frac{e^{-\beta \tilde{E}_0^{(k)0}}}{\tilde{Z}_0^{(k)}} e^{iu(\tilde{E}_l^{\tau_2} - \tilde{E}_0^{(k)0})} + \frac{1}{2} p(k) \frac{e^{-\beta \tilde{E}_1^{(k)0}}}{\tilde{Z}_0^{(k)}} e^{iu(\tilde{E}_l^{\tau_2} - \tilde{E}_1^{(k)0})} \quad (26)$$

The corresponding mixed work PDF is

$$P_B(l, k; W) = \frac{1}{2} p(k) \frac{e^{-\beta \tilde{E}_0^{(k)0}}}{\tilde{Z}_0^{(k)}} \delta[W - (\tilde{E}_l^{\tau_2} - \tilde{E}_0^{(k)0})] + \frac{1}{2} p(k) \frac{e^{-\beta \tilde{E}_1^{(k)0}}}{\tilde{Z}_0^{(k)}} \delta[W - (\tilde{E}_l^{\tau_2} - \tilde{E}_1^{(k)0})] \quad (27)$$

To employ the QDFR with control mismatch for a single history  $(k, l)$  [Eq. (9)] the ratio of forward and backward mixed work PDFs has to be taken. As we did before, we take the ratio of the factors preceding the delta functions. Since in our example the PDF of each  $(k, l)$  history has only two terms, two points are obtained. As there are four possible histories there will be four straight lines as presented in Fig. 13. The QDFR with mismatch implies that the straight lines are given by

$$\ln \frac{P_F(k, l; W)}{P_B(l, k; -W)} = \beta W - \beta \Delta F^{(k)} + I^{(k, l)} \quad (28)$$

From the slope of these straight lines the inverse temperature  $\beta$  can be estimated again (that can be used as a consistency test for the measured data). This estimation is independent of the previous one because the algorithm employed is different. From the same reasoning as before, the work value  $W = \Delta F^{(k)} - \beta^{-1} I^{(k, l)}$  corresponds to the image 1 in the logarithmic plot. If the free-energy differences  $\Delta F^{(k)}$  have been obtained from the analysis without mismatch, the mutual information density  $I^{(k, l)}$  can be estimated from Fig. 13. An independent estimation for the mutual information density could be realized using the circuit in Fig. 8. That circuit provides the joint distribution  $p(k, l)$  from which the mutual information density  $I^{(k, l)} = \ln p(k, l) / (p(k)p(l))$  can be directly computed.

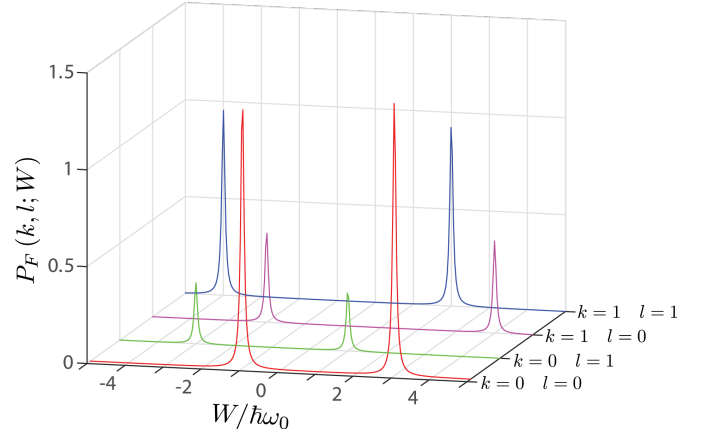


Figure 12. Mixed work PDF with control mismatch,  $P_F(k, l; W)$ . We plotted Lorentz distributions representing the inverse Fourier transformation of some actual experimental data. We used  $\omega_{\tau_2}^{(0)} = 2\omega_0$ ,  $\omega_{\tau_2}^{(1)} = 3\omega_0$ ,  $5\hbar\omega_0 = k_B T$ , and  $\varphi = \pi/3$  in this example.

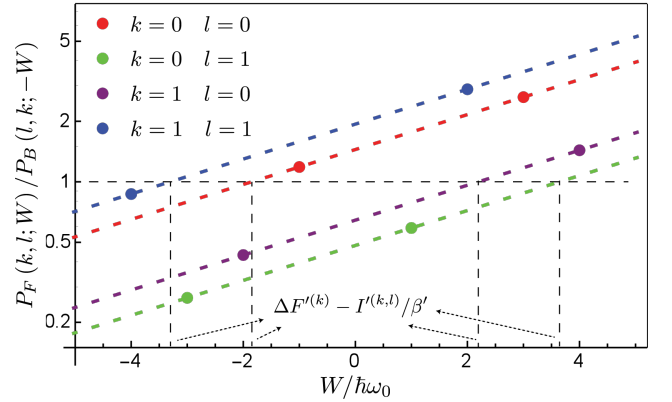


Figure 13. Logarithmic plot of the QDFR for a single history with mismatch. The eight points show the possible transitions which may occur in the forward process if the outcome of the measurement and value of the feedback implemented are, respectively,  $(k=0, l=0)$  (red),  $(k=0, l=1)$  (green),  $(k=1, l=0)$  (purple), and  $(k=1, l=1)$  (blue). The straight lines represent the functions  $\beta W^{(k)} - \beta \Delta F^{(k)} + I^{(k, l)}$ . For each graph one can obtain another estimate for  $\beta$  from their slope. Assuming the knowledge of  $\beta$  and  $\Delta F^{(k)}$ , the mutual information density  $I^{(k, l)}$  is obtained from the work value whose image is 1. Since in our analytical example we plotted the normalized work variable  $W/\hbar\omega_0$ , the slope actually gives  $\beta' = \hbar\omega_0\beta$  and the values whose image is 1 are  $\Delta F^{(k)} + I^{(k, l)}/\beta'$ , where  $\Delta F^{(k)} = \Delta F^{(k)}/\hbar\omega_0$  and  $I^{(k, l)}/\hbar\omega_0$ . We assumed that  $\omega_{\tau_2}^{(0)} = 2\omega_0$ ,  $\omega_{\tau_2}^{(1)} = 3\omega_0$ ,  $5\hbar\omega_0 = k_B T$ , and  $\varphi = \pi/3$ .

Before we proceed with the method, we plotted the forward,  $P_F(W)$ , and backward,  $P_B(W)$ , work PDF in Fig. 14. Without feedback control these PDFs characterize the irreversibility of the process. Here they only characterize the work distribution and thus can be used to obtain the moments of the work stochastic variable,

such as the average work. The irreversibility for processes with feedback is characterized by the joint PDFs,  $P_F(W, \Delta F, I)$  and  $P_B(W, \Delta F, I)$ , which are the quantities that our method is able to obtain from the experimental data.

Hitherto, the method provided several estimates of the inverse temperature  $\beta$ : two possible ways to estimate each free-energy difference  $\Delta F^{(k)}$ , one from the QDFR without mismatch for a single history  $k$  and one in the presence of mismatch (since we have another way to estimate  $I^{(k,l)}$ ), and two estimations of the mutual information density  $I^{(k,l)}$ , one from the QDFR with mismatch for a single history  $(k, l)$  and the other from direct computation using the probability distribution  $p(k, l)$ . With all this information, the final quantities for the verification of the QDFR with feedback control can be computed. Different routes can be chosen depending on which kind of control and information are accessed in a particular experimental setup.

As discussed in the preceding section, the quantities obtained so far are enough to reconstruct the forward and backward joint characteristic functions,  $\chi_F(W, \Delta F, I)$  and  $\chi_B(W, \Delta F, I)$ . The multidimensional inverse Fourier transform of these quantities will give the joint PDFs  $P_F(W, \Delta F, I)$  and  $P_B(W, \Delta F, I)$ , respectively. Each joint PDF will be a sum of delta functions (or Lorentz distributions typically in the experimental analysis) [see Eqs. (G2) and (G4)]. In our example, they contain eight terms. The logarithm of the ratio of these PDFs will provide eight points in a four-dimensional space whose axes are comprised of the work, free-energy difference, and mutual information density random variables. When plotted in logarithmic scale, these points should lie in a

hyperplane in four dimensions given by

$$\ln \frac{P_F(W, \Delta F, I)}{P_B(-W, -\Delta F, I)} = \beta(W - \Delta F) + I. \quad (29)$$

From the experimental data, one would have to use statistical methods to estimate the best hyperplane representing these points.

The coefficients preceding the variables  $W$ ,  $\Delta F$ , and  $I$  in Eq. (29) can be obtained from a multiple linear regression. These values should be  $\beta$ ,  $-\beta$ , and 1, respectively. These values for inverse temperature could be compared to all the independent estimations inferred previously. The fact that the slope in the  $I$  direction is independent of any parameter of the system or the protocol provides a robust consistency test to verify the QDFR.

Some information would necessarily be lost when we plot a projection of this hyperplane associated with Eq. (29) in three dimensions. Therefore, just for the next plot of our example, we assumed that the two gaps in quenched feedback control evolutions are equal, i.e.,  $\omega_{\tau_2}^{(0)} = \omega_{\tau_2}^{(1)} = 2\omega_0$ . In this way, the free-energy difference becomes independent of the feedback  $k$ th protocol,  $\Delta F^{(0)} = \Delta F^{(1)} = \Delta F$ , and the whole feedback process can be fully characterized by a plane in three dimensions. The result of this choice is illustrated in Fig. 15. In that case, where the final gaps are equal but the final Hamiltonians may possibly be different, the coefficients can be estimated as follows. The slope with respect to  $W$  estimates the value of the inverse temperature  $\beta$ . The value of  $\Delta F$  can be obtained by the point of interception of the plane with the  $z$  axis,  $-\beta\Delta F$ , since  $\beta$  was already obtained. The slope with respect to  $I$  should be equal to 1, i.e., independent of any parameter of the protocols. Therefore, the deviation of the slope of  $I$  from 1 is a robust way to verify the QDFR with feedback control.

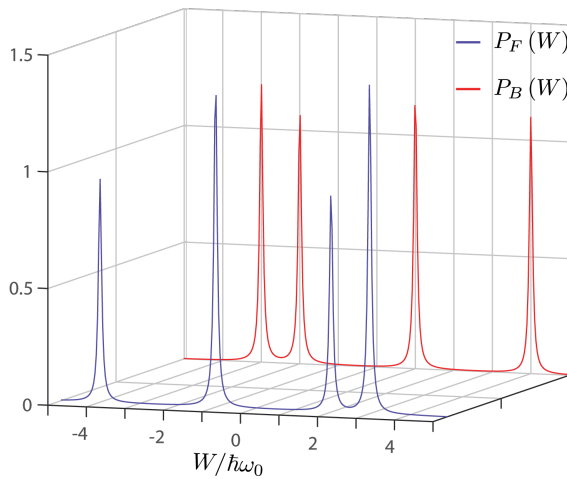


Figure 14. Plot of the forward (red) and backward (blue) work PDFs for the feedback process with control mismatch. We assumed that  $\omega_{\tau_2}^{(0)} = 2\omega_0$ ,  $\omega_{\tau_2}^{(1)} = 3\omega_0$ ,  $5\hbar\omega_0 = k_B T$ , and  $\varphi = \pi/3$ .

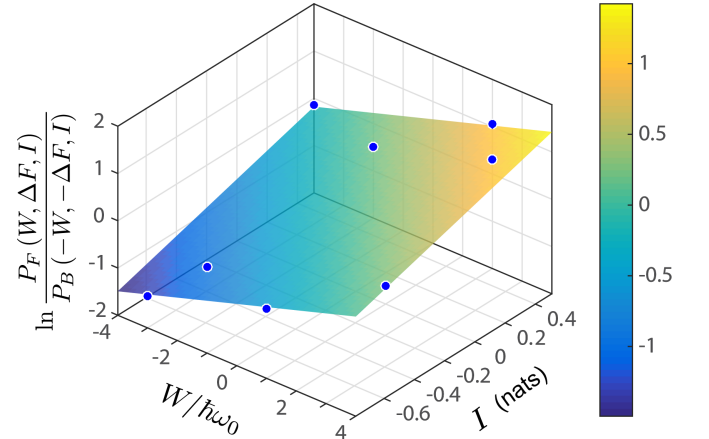


Figure 15. Logarithmic plot of the QDFR for feedback processes. For this plot we assumed  $\omega_{\tau_2}^{(0)} = \omega_{\tau_2}^{(1)} = 2\omega_0$ ,  $5\hbar\omega_0 = k_B T$ , and  $\varphi = \pi/3$ . With these parameters the free energy is independent of the feedback control index  $k$ ,  $\Delta F^{(0)} = \Delta F^{(1)} = \Delta F$ . In this case, the QDFR can be verified by a linear regression technique.

## VI. CONCLUSIONS

We have presented a detailed discussion of the backward protocol and showed that the QDFRs remain valid even when the dynamics is not time-reversal invariant. Our discussion emphasizes that system's external parameters, such as an external magnetic field, should not change under the time-reversal transformation. Furthermore, we derived two QDFRs in the presence of feedback control which apply to each single history after the measurement stage of the control protocol.

Employing the discussed formalism, we also provided a derivation of the QDFR for the whole discrete feedback process. Additionally, we introduced forward and backward mixed joint PDFs. These PDFs incorporate the relevant statistical information of the forward and backward protocols which are instrumental for an experimental verification of QDFRs. The PDFs appearing in the QDFRs can be obtained from these mixed PDFs as marginal distributions. In this sense, the mixed PDFs introduced here provide a unified way to obtain the complete set of PDFs related to the QDFRs in the presence of feedback control. These theoretical developments were applied to obtain our main result.

We proposed a systematic method to experimentally verify the QDFR for discrete feedback-controlled quantum dynamics. The method employs quantum interferometric circuits to measure characteristic functions associated with work distribution in the presence of feedback control. The general strategy involves one ancillary qubit that encodes information of the characteristic function related to a PDF. The feedback mechanism is modeled as a quantum system that carries two quantum memories. Nonetheless, the general ideas introduced throughout the paper can be applied to different feedback control mechanism or to a semiclassical device where the feedback control is processed by classical means.

The QDFRs for feedback processes provide a valuable contribution to quantum information thermodynamics. They quantify the irreversibility of such processes, allowing for generalizations of the second law in the presence of feedback. The algorithm introduced here is experimentally feasible with the current technology for quantum control, for example, in the NMR setup [26, 27, 59, 95, 96] or in a circuit QED setting [75–77]. We hope that our findings inspire new experimental efforts towards a detailed description of the role played by information in the feedback-controlled nonequilibrium quantum dynamics.

## ACKNOWLEDGMENTS

We acknowledge financial support from UFABC, CNPq, CAPES, and FAPESP. R.M.S. gratefully acknowledges financial support from the Royal Society through the Newton Advanced Fellowship scheme (Grant no. NA140436). This research was performed as part of

the Brazilian National Institute of Science and Technology for Quantum Information.

## APPENDIX A. QUANTUM DETAILED FLUCTUATION RELATION WITHOUT FEEDBACK

The work PDF in the driven forward protocol without feedback control may be written as [23, 86]

$$P_F(W) = \sum_{m,n} p(m,n) \delta[W - W_{mn}], \quad (\text{A1})$$

where  $p(m,n) = \text{Tr} [P_m^\tau U_{\tau,0} P_n^0 U_{\tau,0}^\dagger] \text{Tr} [P_n^0 \rho_0^{eq}]$ , with  $\rho_0^{eq} = e^{-\beta(H_0 - F_0)}$ . Introducing identity operators represented in terms of the time-reversal operator,  $\Theta^\dagger \Theta = \mathbb{1}$ , in the expression for the joint distribution  $p(m,n)$ , one obtains

$$p(m,n) = \text{Tr} [\Theta P_m^\tau \Theta^\dagger \Theta U_{\tau,0} \Theta^\dagger \Theta P_n^0 \Theta^\dagger \Theta U_{\tau,0}^\dagger \Theta^\dagger] \times e^{-\beta(E_n^0 - F_0)}, \quad (\text{A2})$$

where we also used  $\text{Tr} [P_n^0 \rho_0^{eq}] = e^{-\beta(E_n^0 - F_0)}$ . Applying the relations between forward and backward protocols discussed in Sec. II, Eq. (A2) can be rewritten as

$$p(m,n) = \text{Tr} [\tilde{P}_n^\tau \tilde{U}_{\tau,0} \tilde{P}_m^0 \tilde{U}_{\tau,0}^\dagger] \text{Tr} [\tilde{P}_m^0 \tilde{\rho}_0^{eq}] \times e^{-\beta(E_n^0 - F_0)} e^{+\beta(\tilde{E}_m^0 - \tilde{F}_0)}, \quad (\text{A3})$$

where we have multiplied and divided by the occupation probability of the initial eigenstates in the backward protocol,  $\tilde{p}(m) = \text{Tr} [\tilde{P}_m^0 \tilde{\rho}_0^{eq}] = e^{-\beta(\tilde{E}_m^0 - \tilde{F}_0)}$ . One can identify the product of the traces in the above equation as the joint probability  $\tilde{p}(n,m)$  of the backward process. Using the relations of the eigenenergies from Sec. II,  $\tilde{E}_m^0 = E_n^\tau$ , and  $\tilde{F}_0 = F_\tau$ , one can write

$$p(m,n) = e^{+\beta(W_{mn} - \Delta F)} \tilde{p}(n,m). \quad (\text{A4})$$

With the above result, Eq. (A1) becomes

$$P_F(W) = \sum_{m,n} e^{+\beta(W_{mn} - \Delta F)} \tilde{p}(m,n) \times \delta[W - W_{mn}]. \quad (\text{A5})$$

Removing the exponential from the sum and using the relation of the eigenenergies again,  $\tilde{W}_{nm} = -W_{mn}$ , we obtain the QDFR

$$P_F(W) = e^{+\beta(W - \Delta F)} \sum_{m,n} \tilde{p}(m,n) \delta[(-W) - \tilde{W}_{nm}] = e^{+\beta(W - \Delta F)} P_B(-W), \quad (\text{A6})$$

without assuming time-reversal invariance of the Hamiltonian.

## APPENDIX B. SINGLE-HISTORY QDFR WITH CONTROL MISMATCH

The forward and backward protocol with control mismatch was discussed in the main text. Here, we describe the steps to demonstrate the QDFR with control mismatch, Eq. (9). The forward mixed joint PDF (introduced in the main text) is given by

$$P_F(k, l; W, \Delta F, I) = \sum_{m, n} p(m^{(k)}, k, l, n) \times \delta[W - W_{mkn}] \delta[\Delta F - \Delta F^{(k)}] \times \delta[I - I^{(k, l)}], \quad (\text{B1})$$

where

$$p(m^{(k)}, k, l, n) = p(m^{(k)}|l) p(k|l) p(l|n) p(n) \quad (\text{B2})$$

are quantities defined previously in the main text. This mixed PDF contains all the relevant statistical information of the forward protocol. By integrating over the proper variables this mixed joint PDF encompasses

$$P_F(k, l) = \iiint dW d(\Delta F) dI P_F(k, l; W, \Delta F, I) = p(k, l), \quad (\text{B3})$$

the joint probability distribution of the  $(k, l)$  history, and

$$P_F(\Delta F) = \sum_{k, l} \iint dW dI P_F(k, l; W, \Delta F, I) = \sum_k p(k) \delta[\Delta F - \Delta F^{(k)}], \quad (\text{B4})$$

the free-energy difference PDF, consistently showing that the probability that the  $k$ th value of the free-energy difference  $\Delta F^{(k)}$  occurs is  $p(k)$ , i.e., the probability that the  $k$ th final Hamiltonian,  $H_{\tau_2}^{(k)}$ , occurs in the feedback protocol. The mutual information density PDF

$$P_F(I) = \sum_{k, l} p(k, l) \delta[I - I^{(k, l)}] \quad (\text{B5})$$

also consistently shows that the probability that the mutual information density,  $I^{(k, l)}$ , occurs is the probability of the  $(k, l)$  history takes place and finally we can write

$$P_F(W) = \sum_{m, k, l, n} p(m^{(k)}, k, l, n) \delta[W - W_{mkn}], \quad (\text{B6})$$

the probability of obtaining the instantaneous eigenenergies difference  $W_{mkn} = E_m^{(k)\tau_2} - E_n^0$  in the TPM scheme. This last PDF is consistent with the forward protocol depicted in Fig. 2, since the average work associated with

it is given by

$$\langle W \rangle = \int dW W P_F(W) = \sum_{k, l} p(k, l) [\mathcal{U}(\rho_{\tau_2}^{(k, l)}) - \mathcal{U}(\rho_0^{eq})]. \quad (\text{B7})$$

The average work for each history  $(k, l)$  is given by the internal energy difference,  $\mathcal{U}(\rho_{\tau_2}^{(k, l)}) - \mathcal{U}(\rho_0^{eq})$  [with  $\mathcal{U}(\rho_{\tau_2}^{(k, l)}) = \text{Tr}(\rho_{\tau_2}^{(k, l)} H_{\tau_2}^{(k)})$  and  $\mathcal{U}(\rho_0^{eq}) = \text{Tr}(\rho_0^{eq} H_0)$ ], and it occurs with probability  $p(k, l)$ . Therefore, the above average work is the mean value over all histories  $(k, l)$  of each single-history average work.

To show the QDFR we employ the forward mixed work PDF

$$P_F(k, l; W) = \sum_{m, n} p(m^{(k)}, k, l, n) \times \delta[W - W_{mkn}]. \quad (\text{B8})$$

Inserting identities,  $\Theta^\dagger \Theta = \mathbb{1}$ , in the expression for the conditional probability for obtaining the  $m$ th instantaneous energy state of  $H_{\tau_2}^{(k)}$  in the  $k$ th history given the  $l$ th outcome in the feedback measurement,  $p(m^{(k)}|l)$ , and the conditional probability for obtaining the  $l$ th outcome in the feedback measurement given the  $n$ th initial energy state,  $p(l|n)$ , one obtains the relation between the forward and backward conditional probabilities

$$p(m^{(k)}|l) = \text{Tr}[\Theta P_m^{(k)\tau_2} \Theta^\dagger \Theta V_{\tau_2, \tau_1}^{(k)} \Theta^\dagger \Theta \mathcal{M}_l \Theta^\dagger \Theta V_{\tau_2, \tau_1}^{(k)\dagger} \Theta^\dagger] = \text{Tr}[\tilde{\mathcal{M}}_l \tilde{V}_{\tilde{\tau}_1, 0}^{(k)} \tilde{P}_m^{(k)0} \tilde{V}_{\tilde{\tau}_1, 0}^{(k)\dagger}] = \tilde{p}(l|m^{(k)}) \quad (\text{B9})$$

and

$$p(l|n) = \text{Tr}[\Theta \mathcal{M}_l \Theta^\dagger \Theta U_{\tau_1, 0} \Theta^\dagger \Theta P_n^0 \Theta^\dagger \Theta U_{\tau_1, 0}^\dagger \Theta] = \text{Tr}[\tilde{P}_n^{\tau_2} \tilde{U}_{\tau_2, \tilde{\tau}_1} \tilde{\mathcal{M}}_l \tilde{U}_{\tau_2, \tilde{\tau}_1}^\dagger] = \tilde{p}(n|l), \quad (\text{B10})$$

where  $\tilde{\tau}_1 = \tau_2 - \tau_1$  and  $\tilde{\mathcal{M}} = \Theta \mathcal{M} \Theta^\dagger$  is the time-reversed observable. Therefore,

$$p(m^{(k)}, k, l, n) = e^{I^{(k, l)}} \frac{p(n)}{\tilde{p}(m^{(k)})} \tilde{p}(l|m^{(k)}) \times \tilde{p}(n|l) \tilde{p}(m^{(k)}) p(k), \quad (\text{B11})$$

where we introduced the probabilities  $\tilde{p}(m^{(k)}) = e^{-\beta(\tilde{E}_m^{(k)0} - \tilde{E}_0^{(k)})}$  and the mutual information density  $I^{(k, l)} = \ln p(k|l)/p(k)$ . Using the relation between forward and backward instantaneous eigenenergies,  $\tilde{E}_n^{(k)t} =$



$E_n^{(k)\tau_2-t}$  and  $\tilde{F}_t^{(k)} = F_{\tau_2-t}^{(k)}$ , the ratio between the initial energy state probabilities will be given by  $p^{(n)}/\tilde{p}^{(m)} = e^{\beta(W_{mkn}-\Delta F^{(k)})}$ . One can identify the remaining probabilities as associated with some backward protocol so that

$$\tilde{p}(n, l, m^{(k)}, k) = \tilde{p}(l|m^{(k)}) \tilde{p}(n|l) \tilde{p}(m^{(k)}) \times p(k). \quad (\text{B12})$$

Therefore,

$$p(m^{(k)}, k, l, n) = e^{\beta(W_{mkn}-\Delta F^{(k)})+I^{(k,l)}} \times \tilde{p}(n, l, m^{(k)}, k). \quad (\text{B13})$$

Substituting Eq. (B13) into Eq. (B8), we obtain

$$P_F(k, l; W) = \sum_{m,n} e^{\beta(W_{mkn}-\Delta F^{(k)})+I^{(k,l)}} \tilde{p}(n, l, m^{(k)}, k) \times \delta[W - W_{mkn}]. \quad (\text{B14})$$

Using the delta function to extract the exponential of work from the sum and identifying the backward mixed work PDF, using  $W_{mkn} = -\tilde{W}_{nkm}$ , we end up with the QDFR written as

$$P_F(k, l; W) = e^{\beta(W-\Delta F^{(k)})+I^{(k,l)}} P_B(l, k; -W), \quad (\text{B15})$$

where

$$P_B(l, k; W) = \sum_{n,m} \tilde{p}(n, l, m^{(k)}, k) \times \delta[W - \tilde{W}_{nkm}]. \quad (\text{B16})$$

The mixed work PDF in Eq. (B16) gives the average work for the backward protocol, which can be written as

$$\begin{aligned} \langle W \rangle &= \sum_{l,k} \int dW W P_B(l, k; W) \\ &= \sum_k p(k) \left\{ \sum_l \tilde{p}(l|k) \left[ \tilde{\mathcal{U}}(\tilde{\rho}_{\tau_2}^{(l,k)}) - \tilde{\mathcal{U}}(\tilde{\rho}_0^{eq,(k)}) \right] \right\}. \end{aligned} \quad (\text{B17})$$

This average work is consistent with the physical description of the backward protocol illustrated in Fig. 3. The difference in the internal energies  $\tilde{\mathcal{U}}(\tilde{\rho}_{\tau_2}^{(l,k)}) - \tilde{\mathcal{U}}(\tilde{\rho}_0^{eq,(k)})$  provides the average work for a single history  $l$  associated with the backward protocol with the  $k$ th initial thermal state  $\tilde{\rho}_0^{eq,(k)}$ . Then, an average over all histories  $l$  is performed, for each  $k$ , by the conditional probability  $\tilde{p}(l|k) = \text{Tr}[\tilde{\mathcal{M}}_l \tilde{V}_{\tau_1,0}^{(k)} \tilde{\rho}_0^{eq,(k)} \tilde{V}_{\tau_1,0}^{(k)\dagger}]$  that the outcome  $l$  occurs given that the system began in  $\tilde{\rho}_0^{eq,(k)}$ . Another average over the initial sampling probability  $p(k)$  is performed in Eq. (B17). This last average corresponds to an

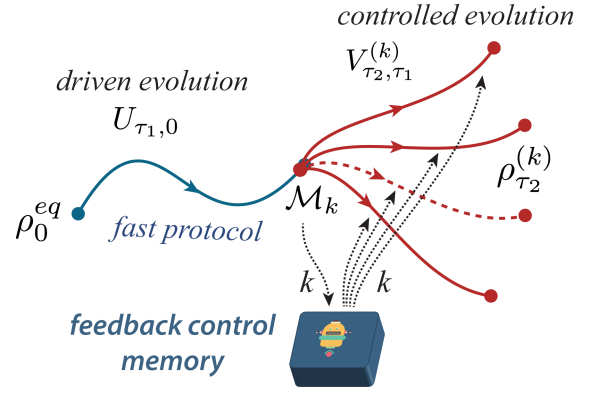


Figure B1. Representation of the forward feedback control protocol without control mismatch. The system starts in thermal equilibrium  $\rho_0^{eq}$  and is driven by external means to the nonequilibrium state  $\rho_{\tau_1}$ . The corresponding evolution operator is  $U_{\tau_1,0}$ . At time  $\tau_1$  an intermediate measurement of some observable  $\mathcal{M}$  is performed. The eigenprojectors of the observable are  $\{\mathcal{M}_k\}$  and the outcome  $k$  is obtained with probability  $q(k)$ . After the measurement the feedback operation  $V_{\tau_2,\tau_1}^{(k)}$  is implemented leading to the Hamiltonian  $H_{\tau_2}^{(k)}$  and final state  $\rho_{\tau_2}^{(k)}$ .

average of the  $k$  distinct protocols which begin with the corresponding Gibbs state  $\tilde{\rho}_0^{eq,(k)}$ . Equation (B17) gives the mean value for the work over all possible histories of the backward protocol.

The backward mixed joint PDF is obtained from the backward mixed work PDF, Eq. (B16), by introducing the free-energy difference and mutual information density delta functions as

$$\begin{aligned} P_B(l, k; W, \Delta F, I) &= \sum_{n,m} \tilde{p}(n, l, m^{(k)}, k) \delta[W - \tilde{W}_{nkm}] \\ &\times \delta[\Delta F - \Delta \tilde{F}^{(k)}] \\ &\times \delta[I - I^{(k,l)}]. \end{aligned} \quad (\text{B18})$$

### APPENDIX C. SINGLE-HISTORY QDFR WITHOUT CONTROL MISMATCH

Here we will discuss the protocol without control mismatch in detail. The forward feedback control protocol is very similar to the case with control mismatch and is depicted in Fig. B1. The only difference is that, without control mismatch, the feedback operation  $V_{\tau_2,\tau_1}^{(k)}$  is always applied to the corresponding outcome  $k$ . The system begins in the thermal state  $\rho_0^{eq} = e^{-\beta H_0}/Z_0$  and evolves under the unitary evolution  $U_{\tau_1,0} = \mathcal{T}_> \exp\{-\frac{i}{\hbar} \int_0^{\tau_1} dt H(t)\}$  up to time  $\tau_1$  and the state evolves to  $\rho_{\tau_1} = U_{\tau_1,0} \rho_0^{eq} U_{\tau_1,0}^\dagger$ . Then, a measurement of the observable  $\mathcal{M}$  is performed, whose eigenprojectors are  $\{\mathcal{M}_k\}$ . After the measurement, the

state changes to  $\rho_{\tau_1}^{(k)} = \mathcal{M}_k \rho_{\tau_1} \mathcal{M}_k / q(k)$  with probability  $q(k) = \text{Tr}[\mathcal{M}_k \rho_{\tau_1}]$ . The feedback operation  $V_{\tau_2 \tau_1}^{(k)} = \mathcal{T}_> \exp \left\{ -\frac{i}{\hbar} \int_{\tau_1}^{\tau_2} dt H^{(k)}(t) \right\}$  leads to the final state  $\rho_{\tau_2}^{(k)} = V_{\tau_2 \tau_1}^{(k)} \rho_{\tau_1}^{(k)} V_{\tau_2 \tau_1}^{(k) \dagger}$  and final Hamiltonian  $H_{\tau_2}^{(k)}$  with probability  $q(k)$ .

Now we introduce the forward mixed PDF

$$P_F^{\text{wcm}}(k; W, \Delta F) = \sum_{m,n} q(m^{(k)}, k, n) \delta[W - W_{mkn}] \times \delta[\Delta F - \Delta F^{(k)}], \quad (\text{C1})$$

where  $q(m^{(k)}, k, n) = q(m^{(k)}|k) q(k|n) p(n)$ , with  $q(m^{(k)}|k) = \text{Tr}[P_m^{(k)\tau_2} V_{\tau_2, \tau_1}^{(k)} \mathcal{M}_k V_{\tau_2, \tau_1}^{(k) \dagger}]$ ,  $q(k|n) = \text{Tr}[\mathcal{M}_k U_{\tau_1, 0} P_n^0 U_{\tau_1, 0}^\dagger]$ , and  $p(n) = e^{-\beta E_n^0} / Z_0$ , is a function of the set of labels  $(m^{(k)}, k, n)$  and  $W_{mkn} = E_m^{(k)\tau_2} - E_n^0$ . This PDF contains the relevant information about energy fluctuations in the protocol. By integrating over all the stochastic variables but one, we consistently obtain the correct marginal probabilities

$$P_F^{\text{wcm}}(k) = \iint dW d(\Delta F) P_F^{\text{wcm}}(k; W, \Delta F) = q(k), \quad (\text{C2})$$

which is the probability of obtaining outcome  $k$  in the intermediate measurement;

$$P_F^{\text{wcm}}(\Delta F) = \sum_k \int dW P_F^{\text{wcm}}(k; W, \Delta F) = \sum_k q(k) \delta[\Delta F - \Delta F^{(k)}], \quad (\text{C3})$$

which correctly reflects the fact that the free energy difference  $\Delta F^{(k)}$  occurs with probability  $q(k)$ ; and

$$P_F^{\text{wcm}}(W) = \sum_{m,n} q(m^{(k)}, k, n) \delta[W - W_{mkn}] = \sum_k q(k) \left[ \mathcal{U}(\rho_{\tau_2}^{(k)}) - \mathcal{U}(\rho_0^{eq}) \right], \quad (\text{C4})$$

which correctly gives the average over histories of the internal energy variation of each history.

We use the same strategy as we did in [APPENDIX B](#) to connect forward and backward protocols. Taking the conditional probabilities  $q(m^{(k)}|k)$  and  $q(k|n)$  and inserting identities, one obtains

$$\begin{aligned} q(m^{(k)}|k) &= \text{Tr} \left[ \Theta P_m^{(k)\tau_2} \Theta^\dagger \Theta V_{\tau_2, \tau_1}^{(k)} \Theta^\dagger \Theta \mathcal{M}_k \Theta^\dagger \Theta V_{\tau_2, \tau_1}^{(k) \dagger} \Theta^\dagger \right] \\ &= \text{Tr} \left[ \tilde{\mathcal{M}}_k \tilde{V}_{\tau_1, 0}^{(k)} \tilde{P}_m^{(k)0} \tilde{V}_{\tau_1, 0}^{(k) \dagger} \right] \\ &= \tilde{q}(k|m^{(k)}) \end{aligned} \quad (\text{C5})$$

and

$$\begin{aligned} q(k|n) &= \text{Tr} \left[ \Theta \mathcal{M}_k \Theta^\dagger \Theta U_{\tau_1, 0} \Theta^\dagger \Theta P_n^0 \Theta^\dagger \Theta U_{\tau_1, 0}^\dagger \Theta \right] \\ &= \text{Tr} \left[ \tilde{P}_n^{\tau_2} \tilde{U}_{\tau_2, \tilde{\tau}_1} \tilde{\mathcal{M}}_k \tilde{U}_{\tau_2, \tilde{\tau}_1}^\dagger \right] \\ &= \tilde{q}(n|k), \end{aligned} \quad (\text{C6})$$

where  $\tilde{\tau}_1 = \tau_2 - \tau_1$  and  $\tilde{\mathcal{M}} = \Theta \mathcal{M} \Theta^\dagger$  is the time-reversed observable. We also have multiplied and divided by the probability  $\tilde{p}(m^{(k)}) = \text{Tr}[\tilde{P}_m^{(k)0} \tilde{\rho}_0^{eq, (k)}] = e^{-\beta(\tilde{E}_m^{(k)0} - \tilde{F}_0^{(k)})}$  of having the initial eigenenergies of the backward process with initial Gibbs state  $\tilde{\rho}_0^{eq, (k)} = e^{-\beta \tilde{H}_0^{(k)}} / \tilde{Z}_0^{(k)}$ . All together, these calculations will give

$$\begin{aligned} q(m^{(k)}, k, n) &= \tilde{q}(n|k) \tilde{q}(k|m^{(k)}) \tilde{p}(m^{(k)}) \\ &\times e^{-\beta(E_n^0 - F_0)} e^{+\beta(\tilde{E}_m^{(k)0} - \tilde{F}_0^{(k)})}. \end{aligned} \quad (\text{C7})$$

We identify the product in the first line of Eq. (C7) as  $\tilde{q}(n, k, m^{(k)}) = \tilde{q}(n|k) \tilde{q}(k|m^{(k)}) \tilde{p}(m^{(k)})$ , which will be associated to the backward protocol in a moment. The term in the second line of Eq. (C7) can be written as  $e^{+\beta(W_{mkn} - \Delta F^{(k)})}$ . Therefore, the mixed work PDF, obtained by integrating over  $\Delta F$  in Eq. (C1), can be written as

$$P_F^{\text{wcm}}(k; W) = \sum_{m,n} e^{+\beta(W_{mkn} - \Delta F^{(k)})} \tilde{q}(n, k, m^{(k)}) \times \delta[W - W_{mkn}]. \quad (\text{C8})$$

Using the delta function and identifying the associated backward work PDF, we arrive at the single-history QDFR without control mismatch

$$P_F^{\text{wcm}}(k; W) = e^{+\beta(W - \Delta F^{(k)})} P_B^{\text{wcm}}(k; -W), \quad (\text{C9})$$

where

$$\begin{aligned} P_B^{\text{wcm}}(k; W) &= \sum_{n,m} \tilde{q}(n, k, m^{(k)}) \\ &\times \delta[W - \tilde{W}_{nkm}]. \end{aligned} \quad (\text{C10})$$

The backward work PDF  $P_B^{\text{wcm}}(W) = \sum_k P_B^{\text{wcm}}(k; W)$  does not provide another backward protocol as one would have expected. The average work of the backward work PDF,  $\int dW W P_B^{\text{wcm}}(W)$ , cannot be interpreted as the average over histories of the work of some TPM protocol. This could call into question the validity of  $P_B^{\text{wcm}}(W)$  as a PDF. However,  $P_B^{\text{wcm}}(W)$  is always nonnegative and normalized, i.e.,  $\int dW P_B^{\text{wcm}}(W) = 1$ . Based on these properties, we have chosen to still call it a PDF, although it lacks a proper protocol associated with it in the absence of control mismatch.

From a pragmatic point of view, the function  $P_B^{\text{wcm}}(k; W)$  provides a fluctuation relation and its Fourier transform can be experimentally measured. Even if one choses to not call it a PDF, this quantity can be measured and it is instrumental in our method.

#### APPENDIX D. WHOLE-PROCESS QDFR FOR FEEDBACK CONTROL

From the mixed joint PDF, Eq. (B1), we obtain the joint PDF by summing over the discrete variables  $k$  and  $l$ . This gives

$$\begin{aligned} P_F(W, \Delta F, I) &= \sum_{k,l} P_F(k, l; W, \Delta F, I) \\ &= \sum_{m,k,l,n} p(m^{(k)}, k, l, n) \delta[W - W_{mkn}] \\ &\quad \times \delta[\Delta F - \Delta F^{(k)}] \delta[I - I^{(k,l)}]. \end{aligned} \quad (\text{D1})$$

We use the relation between forward and backward protocols and introduce conveniently identities inside the definition of  $p(m^{(k)}, k, l, n)$ . This calculation was already performed and the result was given in Eq. (B13). Therefore,

$$\begin{aligned} P_F(W, \Delta F, I) &= \sum_{m,k,l,n} e^{\beta(W_{mkn} - \Delta F^{(k)}) + I^{(k,l)}} \\ &\quad \times \tilde{p}(n, l, m^{(k)}, k) \delta[W - W_{mkn}] \\ &\quad \times \delta[\Delta F - \Delta F^{(k)}] \delta[I - I^{(k,l)}]. \end{aligned} \quad (\text{D2})$$

Using the delta functions to remove the exponential from the summation symbol and identifying the remainder term as the backward joint PDF, we arrive at the QDFR

$$P_F(W, \Delta F, I) = e^{\beta(W - \Delta F) + I} P_B(-W, -\Delta F, I), \quad (\text{D3})$$

where the three variables  $W$ ,  $\Delta F$ , and  $I$  are stochastic and

$$\begin{aligned} P_B(W, \Delta F, I) &= \sum_{n,l,m,k} \tilde{p}(n, l, m^{(k)}, k) \delta[W - \tilde{W}_{nkm}] \\ &\quad \times \delta[\Delta F - \Delta \tilde{F}^{(k)}] \delta[I - I^{(k,l)}] \end{aligned} \quad (\text{D4})$$

is the backward joint PDF, which can be obtained from Eq. (B18) by summing over  $k$  and  $l$ .

#### APPENDIX E. CHARACTERISTIC FUNCTIONS

As mentioned in the main text, the four characteristic functions relevant for our method are:  $\chi_F^{(k,l)}(u)$ ,  $\chi_B^{(l,k)}(u)$ ,  $\chi_F^{\text{wcm}(k)}(u)$ , and  $\chi_B^{\text{wcm}(k)}(u)$ , which are the Fourier transform of the work variable of the mixed work PDFs,  $P_F(k, l; W)$ ,  $P_B(l, k; W)$ ,  $P_F^{\text{wcm}}(k; W)$ , and  $P_B^{\text{wcm}}(k; W)$ , respectively. These calculations are reasonably easy to perform. We explicitly wrote the result of the forward and backward characteristic functions with control mismatch in the main text [see Eqs. (15) and (16)]. For the sake of completeness, in this appendix we write explicitly the characteristic functions without control mismatch. The forward and backward characteristic functions without control mismatch are respectively given by

$$\begin{aligned} \chi_F^{\text{wcm}(k)}(u) &= \int dW P_F^{\text{wcm}}(k; W) e^{iuW} \\ &= \text{Tr} \left[ e^{+iuH_{\tau_2}^{(k)}} V_{\tau_2, \tau_1}^{(k)} \mathcal{M}_k U_{\tau_1, 0} e^{-iuH_0} \rho_0^{eq} U_{\tau_1, 0}^\dagger \mathcal{M}_k V_{\tau_2, \tau_1}^{(k)\dagger} \right], \end{aligned} \quad (\text{E1})$$

$$\begin{aligned} \chi_B^{\text{wcm}(k)}(u) &= \int dW P_B^{\text{wcm}}(k; W) e^{iuW} \\ &= \text{Tr} \left[ e^{+iu\tilde{H}_{\tau_2}} \tilde{U}_{\tau_2, \tilde{\tau}_1} \tilde{\mathcal{M}}_k \tilde{V}_{\tilde{\tau}_1, 0}^{(k)} e^{-iu\tilde{H}_0^{(k)}} \tilde{\rho}_0^{eq, (k)} \tilde{V}_{\tilde{\tau}_1, 0}^{(k)\dagger} \tilde{\mathcal{M}}_k \tilde{U}_{\tau_2, \tilde{\tau}_1} \right]. \end{aligned} \quad (\text{E2})$$

#### APPENDIX F. QUANTUM INTERFEROMETRIC CIRCUITS

Each interferometric circuit in the main text was designed to encode, in an auxiliary qubit, all the information necessary to reconstruct the characteristic function of interest, providing a full characterization of energy fluctuations in a quantum feedback protocol. Let  $\mathcal{M}$  be the observable in the feedback protocol and  $\{\mathcal{M}_k\}$  its eigenprojectors set. The first CNOT gate in Fig. 5 and

the CNOT gate in Fig. 6 are not the usual CNOT gates. The control basis is not the computational basis but the basis composed by the eigenprojectors of the observable of the feedback protocol. The  $\mathcal{M}$ -CNOT gate will be defined as

$$\mathcal{M}_0^S \otimes \mathbb{1}^M + \mathcal{M}_1^S \otimes \sigma_x^M. \quad (\text{F1})$$

The target qubit  $M$  is flipped when the system's state is associated with the outcome 1 (projector  $\mathcal{M}_1^S$ ). As the memory starts in the reference state  $|0^M\rangle$ , the mem-

ory state will remain the same if the system is in state  $\mathcal{M}_0$  and will flip to  $|1^M\rangle$  if the system is in state  $\mathcal{M}_1$ . Therefore, this gate correlates the system and memory states; two of the diagonal elements of the resulting state in the  $\mathcal{M}^S \otimes \sigma_z^M$  basis will be  $\mathcal{M}_k^S \otimes |k^M\rangle \langle k^M|$  weighted by the corresponding probability of measuring the outcome  $k$ . It is important to note that this protocol can be generalized for a system with higher dimensions; in this case the feedback memory system should have the same dimension as the system of interest.

The algorithm in Fig. 5 is used to obtain the characteristic function  $\chi_F^{(k,l)}(u)$ . The measurement of the two memories is necessary, i.e., one is related to the outcome of the feedback measurement and the other is related to the feedback operation implemented. The probability of obtaining the outcome pair  $(k, l)$  is given by

$$p^{M_1 M_2}(k, l) = \frac{1}{2} p(k|l) \sum_{i=1,2} \text{Tr}[B_{ki} V_{\tau_2, \tau_1}^{(k)} \mathcal{M}_l U_{\tau_1, 0} W_i \times \rho_0^{eq, (k)} W_i^\dagger U_{\tau_1, 0}^\dagger \mathcal{M}_l V_{\tau_2, \tau_1}^{(k)\dagger} B_{ki}^\dagger], \quad (\text{F2})$$

where  $W_0 = e^{-iuH_0}$ ,  $W_1 = \mathbb{1}$ ,  $B_{00} = B_{10} = \mathbb{1}$ ,  $B_{k1} = e^{-iuH_{\tau_2}^{(k)}}$ , and  $p(k|l) = |\langle k | R_x(\varphi) | l \rangle|^2$ .

The algorithm in Fig. 6 is used to measure the characteristic function  $\chi_F^{\text{wcm}(k)}(u)$ . In this case, the measurement of a single memory, related to the outcome of the feedback measurement, is necessary. The probability of obtaining the outcome  $k$  is given by

$$p^M(k) = \frac{1}{2} \sum_{i=1,2} \text{Tr}[B_{ki} V_{\tau_2, \tau_1}^{(k)} \mathcal{M}_k U_{\tau_1, 0} W_i \times \rho_0^{eq} W_i^\dagger U_{\tau_1, 0}^\dagger \mathcal{M}_k V_{\tau_2, \tau_1}^{(k)\dagger} B_{ki}^\dagger], \quad (\text{F3})$$

where  $W_i$  and  $B_{kl}$  were defined in the previous paragraph.

## APPENDIX G. DETAILS ABOUT THE ANALYTICAL EXAMPLE

In this appendix we show the explicit expressions for the forward and backward joint PDFs  $P_F(W, \Delta F, I)$  and  $P_B(W, \Delta F, I)$ , respectively. The forward joint characteristic function,  $\chi_F(u, v, w)$ , is given by Eq. (15), whereas the forward work characteristic function,  $\chi_F^{(k,l)}(u)$ , for our example is given by Eq. (24). The PDF is obtained from the inverse Fourier transform of the respective char-

The algorithm in Fig. 8 is used to measure the trace  $\mathcal{A}(k, l)$  defined in Sec. III B [see Eq. (16)]. This trace comprised part of the characteristic function with mismatch  $\chi_B^{(l,k)}(u) = p(k) \mathcal{A}(k, l)$  and gives the characteristic function without mismatch  $\chi_B^{\text{wcm}(k)}(u) = \mathcal{A}(k, k)$ . The probability of the memory measurement is given by

$$p_B^M(l) = \frac{1}{2} \sum_{i=1,2} \text{Tr}[A_i \tilde{U}_{\tau_2, \tilde{\tau}_1} \tilde{\mathcal{M}}_l \tilde{V}_{\tilde{\tau}_1, 0}^{(k)} W_i^{(k)} \times \rho_0^{eq, (k)} W_i^{(k)\dagger} \tilde{V}_{\tilde{\tau}_1, 0}^{(k)\dagger} \tilde{\mathcal{M}}_l \tilde{U}_{\tau_2, \tilde{\tau}_1}^\dagger A_i^\dagger], \quad (\text{F4})$$

where  $W_0^{(k)} = e^{-i\tilde{H}_0^{(k)}}$ ,  $W_1^{(k)} = A_0 = \mathbb{1}$ , and  $A_1 = e^{-iu\tilde{H}_{\tau_2}}$ . After the memory measurement with an outcome  $l$  the matrix element  $\langle 0^A | \rho_l^A | 1^A \rangle$  of the ancilla state at the end of the circuit is given by

$$\langle 0^A | \rho_l^A | 1^A \rangle = \frac{1}{2p_B^M(l)} \mathcal{A}(k, l). \quad (\text{F5})$$

Therefore, we can see that if the outcome is  $l = k$ , then  $\langle 0^A | \rho_{l=k}^A | 1^A \rangle = \chi_B^{\text{wcm}(k)}(u) / 2p_B^M(l = k)$ . The averages  $\langle \sigma_x^A \rangle = \text{Re}[\chi_B^{\text{wcm}(k)}(u)] / p_B^M(l = k)$  and  $\langle \sigma_y^A \rangle = \text{Im}[\chi_B^{\text{wcm}(k)}(u)] / p_B^M(l = k)$  will provide the real and imaginary parts of the work characteristic function, respectively. For an arbitrary  $l$ , the averages of the ancilla Pauli operators will be  $\langle \sigma_x^A \rangle = \text{Re}[\mathcal{A}(k, l)] / p_B^M(l)$  and  $\langle \sigma_y^A \rangle = \text{Im}[\mathcal{A}(k, l)] / p_B^M(l)$ . Hence,  $\mathcal{A}(k, l)$  can be constructed and part of  $\chi_B^{(l,k)}(u)$  is obtained.

For the sake of clarity, Fig. F1 displays an alternative way to understand the whole strategy to verify the detailed fluctuation relation for feedback-controlled quantum systems.

acteristic function

$$P_F(W, \Delta F, I) = \frac{1}{(2\pi)^3} \iiint_{-\infty}^{\infty} du dv dw \times e^{-i(uW + v\Delta F + wI)} \chi_F(u, v, w). \quad (\text{G1})$$

Substituting  $\chi_F^{(k,l)}(u)$  into  $\chi_F(u, v, w)$  and evaluating the integrals, we obtain



	Measured from the interferometric circuits	Obtained from inverse Fourier transform	QDFR employed	Estimated from the QDFR
Without control mismatch	$\chi_F^{\text{wcm}(k)}(u)$	$P_F^{\text{wcm}}(k; W)$	Eq. (23) $\ln \frac{P_F^{\text{wcm}}(k; W)}{P_B^{\text{wcm}}(k; -W)} = \beta W - \beta \Delta F^{(k)}$	$\beta$ (Independently estimated) $\Delta F^{(k)}$
	$\chi_B^{\text{wcm}(k)}(u)$	$P_B^{\text{wcm}}(k; W)$		
With control mismatch	$\chi_F^{(k,l)}(u)$	$P_F(k, l; W)$	Eq. (28) $\ln \frac{P_F(k, l; W)}{P_B(l, k; -W)} = \beta W - \beta \Delta F^{(k)} + I^{(k,l)}$	$\beta$ (estimated) $I^{(k,l)}$
	$\chi_B^{(l,k)}(u)$	$P_B(l, k; W)$		

From the measured quantities,  $\chi_F^{(k,l)}(u)$  and  $\chi_B^{(l,k)}(u)$ , and the estimated ones,  $\beta$ ,  $\Delta F^{(k)}$  and  $I^{(k,l)}$ , we can reconstruct the whole-history characteristic functions and consequently verify the QDFR using multilinear regression.

Whole QDFR	$\chi_F(u, v, w)$	$P_F(W, \Delta F, I)$	Eq. (29) $\ln \frac{P_F(W, \Delta F, I)}{P_B(-W, -\Delta F, I)} = \beta(W - \Delta F) + I$	$\beta$ $\Delta F^{(k)}$
	$\chi_B(u, v, w)$	$P_B(W, \Delta F, I)$		$I^{(k,l)}$

Can be independently estimated from the circuit in Fig. 7

Figure F1. In order to verify the QDFR [Eq. (13) or (29)] the two measured characteristic functions,  $\chi_F^{(k,l)}(u)$  and  $\chi_B^{(l,k)}(u)$ , and the three estimated quantities,  $\beta$ ,  $\Delta F^{(k)}$ , and  $I^{(k,l)}$ , are necessary. Given the estimated quantities, the procedure to verify the QDFR is the same: Constructing the characteristic functions  $\chi_F(u, v, w)$  and  $\chi_B(u, v, w)$  from the measured data, one obtains the corresponding joint PDFs by inverse Fourier transform and then applies multilinear regression to the set of points corresponding to the ratio of the PDFs in logarithmic scale. On the other hand, there are two pathways to obtain the estimated quantities ( $\beta$ ,  $\Delta F^{(k)}$ , and  $I^{(k,l)}$ ). These two pathways are indicated by blue and red arrows in the sketched table. In any case, the inverse temperature  $\beta$  is always estimated independently. From the blue pathway one obtains first the free-energy differences  $\Delta F^{(k)}$  from the QDFR given by Eq. (11) or (23) and uses such quantities to obtain the mutual information density from the other QDFR in Eq. (9) or (28). This pathway was employed in the analytical example discussed in Sec. V. In the red pathway, we obtain the mutual information density first, through the measurement of the joint probability  $p(k, l)$  employing the circuit in Fig. 8. With the joint probability  $p(k, l)$ , the mutual information density can be calculated and then employed to estimate the free-energy differences using the QDFR of Eq. (9) or (28).

$$P_F(W, \Delta F, I) = \sum_{k,l} \frac{1}{2} p(k|l) \frac{e^{-\beta E_l^0}}{Z_0} \left\{ \delta \left[ W - \left( E_1^{(k, \tau_2)} - E_l^0 \right) \right] + \delta \left[ W - \left( E_0^{(k, \tau_2)} - E_l^0 \right) \right] \right\} \\ \times \delta \left[ \Delta F - \Delta F^{(k)} \right] \delta \left[ I - I^{(k,l)} \right]. \quad (\text{G2})$$

Since  $k$  and  $l$  have two possible values, there are eight peaks in the stochastic variable space  $(W, \Delta F, I)$ . The forward work PDF, plotted in Fig. 14, can be easily obtain by integrating over the free-energy difference and mutual information density.

The backward joint characteristic function,  $\chi_B(u, v, w)$ , is given by Eq. (18), whereas the backward work characteristic function,  $\chi_B^{(l,k)}(u)$ , is given by Eq. (26). The backward joint PDF is obtained from the

inverse Fourier transform of the respective characteristic function

$$P_B(W, \Delta F, I) = \frac{1}{(2\pi)^3} \iiint_{-\infty}^{\infty} du dv dw \\ \times e^{-i(uW + v\Delta F + wI)} \chi_B(u, v, w). \quad (\text{G3})$$

Substituting  $\chi_B^{(l,k)}(u)$  into  $\chi_B(u, v, w)$  and evaluating the integrals, we obtain

$$P_B(W, \Delta F, I) = \sum_{l,k} \frac{1}{2} p(k) \frac{e^{-\beta \tilde{E}_0^{(k)0}}}{\tilde{Z}_0^{(k)}} \left\{ \delta \left[ W - \left( \tilde{E}_l^{\tau_2} - \tilde{E}_0^{(k)0} \right) \right] + \delta \left[ W - \left( \tilde{E}_l^{\tau_2} - \tilde{E}_1^{(k)0} \right) \right] \right\} \\ \times \delta \left[ \Delta F - \Delta \tilde{F}^{(k)} \right] \delta \left[ I - I^{(k,l)} \right]. \quad (\text{G4})$$

The backward work PDF plotted in Fig. 14 can be easily

obtain by integrating over the free-energy difference and mutual information density.

- 
- [1] J. C. Maxwell, On Governors, Proc. R. Soc. **16**, 270 (1867).
  - [2] C.-G. Kang, Origin of Stability Analysis: “On Governors” by J.C. Maxwell [Historical Perspectives], IEEE Control Systems **36**, 77 (2016).
  - [3] J. Bechhoefer, Feedback for physicists: A tutorial essay on control, Rev. Mod. Phys. **77**, 783 (2005).
  - [4] K. Jacobs, Applications of Feedback Control in Quantum Systems, arXiv:quant-ph/0605015v1 (2006).
  - [5] J. Zhang, Y.-X. Liu, R.-B. Wu, K. Jacobs, and F. Nori, Quantum feedback: theory, experiments, and applications, Phys. Rep. **679**, 1 (2017).
  - [6] H. S. Leff and A. F. Rex, *Maxwell’s Demon 2 Entropy, Classical and Quantum Information, Computing* (IOP Publishing, Bristol, 2003), 2nd edition.
  - [7] K. Maruyama, F. Nori, and V. Vedral, Colloquium: The physics of Maxwell’s demon and information, Rev. Mod. Phys. **81**, 1 (2009).
  - [8] E. Lutz and S. Ciliberto, Information: From Maxwell’s demon to Landauer’s eraser, Physics Today **68**, 30 (2015).
  - [9] E. Jaynes, Information Theory and Statistical Mechanics, Phys. Rev. **106**, 620 (1957).
  - [10] E. Jaynes, Information Theory and Statistical Mechanics II, Phys. Rev. **108**, 171 (1957).
  - [11] C. Jarzynski, Equalities and inequalities: Irreversibility and the second law of thermodynamics at the nanoscale, Annu. Rev. Condens. Matter Phys. **2**, 329 (2011).
  - [12] R. Klages, W. Just and C. Jarzynski, *Nonequilibrium Statistical Physics of Small Systems, Fluctuation Relations and Beyond* (Wiley-VCH, Weinheim, 2013).
  - [13] S. Vinjanampathy and J. Anders, Quantum thermodynamics, Contemp. Phys. **57**, 545 (2016).
  - [14] J. Millen and A. Xuereb, Perspective on quantum thermodynamics, New J. Phys. **18**, 011002 (2016).
  - [15] D. Gelbwaser-Klimovsky, W. Niedenzu, and G. Kurizki, Chapter Twelve - Thermodynamics of Quantum Systems Under Dynamical Control, Adv. At. Mol. Opt. Phys. **64**, 329 (2015).
  - [16] M. Esposito, Nonequilibrium fluctuations, fluctuation theorems, and counting statistics in quantum systems, Rev. Mod. Phys. **81**, 1665 (2009).
  - [17] U. Seifert, Stochastic thermodynamics, fluctuation theorems and molecular machines, Rep. Prog. Phys. **75**, 126001 (2012).
  - [18] C. Jarzynski, Nonequilibrium Equality for Free Energy Differences, Phys. Rev. Lett. **78**, 2690 (1997).
  - [19] C. Jarzynski, Equilibrium free-energy differences from nonequilibrium measurements: A master-equation approach, Phys. Rev. E **56**, 5018 (1997).
  - [20] G. E. Crooks, Entropy production fluctuation theorem and the nonequilibrium work relation for free energy differences, Phys. Rev. E **60**, 2721 (1999).
  - [21] H. Tasaki, Jarzynski Relations for Quantum Systems and Some Applications, arXiv:cond-mat/0009244v2 (2000).
  - [22] J. Kurchan, A Quantum Fluctuation Theorem, arXiv:cond-mat/0007360v2 (2001).
  - [23] M. Campisi, P. Hänggi, and P. Talkner, Colloquium: Quantum fluctuation relations: Foundations and applications, Rev. Mod. Phys. **83**, 771 (2011).
  - [24] P. Hänggi and P. Talkner, The other QFT, Nat. Phys. **11**, 108 (2015).
  - [25] W. L. Ribeiro, G. T. Landi, and F. L. Semião, Quantum thermodynamics and work fluctuations with applications to magnetic resonance, Am. J. Phys. **84**, 948 (2016).
  - [26] T. B. Batalhão, A. M. Souza, L. Mazzola, R. Auccaise, R. S. Sarthour, I. S. Oliveira, J. Goold, G. De Chiara, M. Paternostro, and R. M. Serra, Experimental Reconstruction of Work Distribution and Study of Fluctuation Relations in a Closed Quantum System, Phys. Rev. Lett. **113**, 140601 (2014).
  - [27] T. B. Batalhão, A. M. Souza, R. S. Sarthour, I. S. Oliveira, M. Paternostro, E. Lutz, and R. M. Serra, Irreversibility and the Arrow of Time in a Quenched Quantum System, Phys. Rev. Lett. **115**, 190601 (2015).
  - [28] S. An, J.-N. Zhang, M. Um, D. Lv, Y. Lu, J. Zhang, Z.-Q. Yin, H. T. Quan, and K. Kim, Experimental test of the quantum Jarzynski equality with a trapped-ion system, Nat. Phys. **11**, 193 (2015).
  - [29] M. Naghiloo, D. Tan, P. M. Harrington, J. J. Alonso, E. Lutz, A. Romito, and K. W. Murch, Thermodynamics along individual trajectories of a quantum bit, arXiv:1703.05885 (2017).
  - [30] A. Smith, Y. Lu, S. An, X. Zhang, J.-N. Zhang, Z. Gong, H. T. Quan, C. Jarzynski, and K. Kim, Verification of the quantum nonequilibrium work relation in the presence of decoherence, New J. Phys. **20**, 013008 (2018).
  - [31] R. Medeiros de Araújo, T. Häffner, R. Bernardi, D. S. Tasca, M. P. J. Lavery, M. J. Padgett, A. Kanaan, L. C. Céleri, and P. H. Souto Ribeiro, Experimental study of quantum thermodynamics using optical vortices, J. Phys. Commun. **2**, 035012 (2018).
  - [32] S. Lloyd, Quantum-mechanical Maxwell’s demon, Phys. Rev. A **56**, 3374 (1997).
  - [33] T. Sagawa, *Thermodynamics of Information Processing in Small Systems* (Springer Theses, Springer, New York, 2012).
  - [34] J. M. R. Parrondo, J. M. Horowitz, and T. Sagawa, Thermodynamics of information, Nat. Phys. **11**, 131 (2015).
  - [35] A. Chapman and A. Miyake, How an autonomous quantum Maxwell demon can harness correlated information, Phys. Rev. E **92**, 062125 (2015).
  - [36] K. Brandner, M. Bauer, M. T. Schmid, and U. Seifert, Coherence-enhanced efficiency of feedback-driven quantum engines, New J. Phys. **17**, 065006 (2015).
  - [37] D. Girolami, R. Schmidt, and G. Adesso, Towards quantum cybernetics, Ann. Phys. **527**, 757 (2015).
  - [38] P. Kammerlander and J. Anders, Coherence and measurement in quantum thermodynamics, Sci. Rep. **6**, 22174 (2016).
  - [39] A. V. Lebedev, D. Oehri, G. B. Lesovik, and G. Blatter, Trading coherence and entropy by a quantum Maxwell demon, Phys. Rev. A **94**, 052133 (2016).
  - [40] A. Kutvonen, T. Sagawa, and T. Ala-Nissila, Thermo-

- dynamics of information exchange between two coupled quantum dots, *Phys. Rev. E* **93**, 032147 (2016).
- [41] M. Weilenmann, L. Kraemer, P. Faist, and R. Renner, Axiomatic Relation between Thermodynamic and Information-Theoretic Entropies, *Phys. Rev. Lett.* **117**, 260601 (2016).
  - [42] C. Elouard, D. Herrera-Martí, M. Clusel, and A. Auffèves, The role of quantum measurement in stochastic thermodynamics, *npj Quantum Inf.* **3**, 1 (2017).
  - [43] P. Strasberg, G. Schaller, T. Brandes, and M. Esposito, Quantum and Information Thermodynamics: A Unifying Framework based on Repeated Interactions, *Phys. Rev. X* **7**, 021003 (2017).
  - [44] C. Elouard, D. Herrera-Martí, B. Huard, and Alexia Auffèves, Extracting work from quantum measurements in Maxwell's demon engines, *Phys. Rev. Lett.* **118**, 260603 (2017).
  - [45] A. Shu, J. Dai, and V. Scarani, Power of an optical Maxwell's demon in the presence of photon-number correlations, *Phys. Rev. A* **95**, 022123 (2017).
  - [46] T. Sagawa and M. Ueda, Jarzynski Equality with Maxwell's Demon, *arXiv:cond-mat/0609085v3* (2006).
  - [47] T. Sagawa and M. Ueda, Second Law of Thermodynamics with Discrete Quantum Feedback Control, *Phys. Rev. Lett.* **100**, 080403 (2008).
  - [48] T. Sagawa and M. Ueda, Generalized Jarzynski Equality under Nonequilibrium Feedback Control, *Phys. Rev. Lett.* **104**, 090602 (2010).
  - [49] Y. Morikuni and H. Tasaki, Quantum Jarzynski-Sagawa-Ueda Relations, *J. Stat. Phys.* **143**, 1 (2011).
  - [50] T. Sagawa and M. Ueda, Fluctuation Theorem with Information Exchange: Role of Correlations in Stochastic Thermodynamics, *Phys. Rev. Lett.* **109**, 180602 (2012).
  - [51] S. Lahiri, S. Rana, and A. M. Jayannavar, Fluctuation theorems in the presence of information gain and feedback, *J. Phys. A: Math. Theor.* **45**, 065002 (2012).
  - [52] K. Funo, Y. Watanabe, and M. Ueda, Integral quantum fluctuation theorems under measurement and feedback control, *Phys. Rev. E* **88**, 052121 (2013).
  - [53] C. A. Fuchs and K. Jacobs, Information-tradeoff relations for finite-strength quantum measurements, *Phys. Rev. A* **63**, 062305 (2001).
  - [54] F. Buscemi, M. Hayashi, and M. Horodecki, Global information balance in quantum measurements, *Phys. Rev. Lett.* **100**, 210504 (2008).
  - [55] F. Buscemi, and M. Horodecki, Towards a Unified Approach to Information-Disturbance Tradeoffs in Quantum Measurements, *Open Syst. Inf. Dyn.* **16**, 29 (2009).
  - [56] M. Berta, J. M. Renes, and M. M. Wilde, Identifying the Information Gain of a Quantum Measurement, *IEEE Trans. Inf. Theory* **60**, 7987 (2014).
  - [57] K. Jacobs, *Quantum Measurement Theory and its Application* (Cambridge University Press, Cambridge, 2014).
  - [58] R. Kosloff, Quantum thermodynamics: A dynamical viewpoint, *Entropy* **15**, 2100 (2013).
  - [59] P. A. Camati, J. P. S. Peterson, T. B. Batalhão, K. Micadei, A. M. Souza, R. S. Sarthour, I. S. Oliveira, and R. M. Serra, Experimental rectification of entropy production by a Maxwell's Demon in a quantum system, *Phys. Rev. Lett.* **117**, 240502 (2016).
  - [60] T. M. Cover, and J. A. Thomas, *Elements of Information Theory* (John Wiley & Sons, Inc., Hoboken, 2006), 2nd edition.
  - [61] H. Tajima, Second law of information thermodynamics with entanglement transfer, *Phys. Rev. E* **88**, 042143 (2013).
  - [62] L. Mazzola, G. De Chiara, and M. Paternostro, Measuring the Characteristic Function of the Work Distribution, *Phys. Rev. Lett.* **110**, 230602 (2013).
  - [63] R. Dornier, S. R. Clark, L. Heaney, R. Fazio, J. Goold, and V. Vedral, Extracting Quantum Work Statistics and Fluctuation Theorems by Single-Qubit Interferometry, *Phys. Rev. Lett.* **110**, 230601 (2013).
  - [64] S. Toyabe, T. Sagawa, M. Ueda, E. Muneyuki, and M. Sano, Experimental demonstration of information-to-energy conversion and validation of the generalized Jarzynski equality, *Nat. Phys.* **6**, 988 (2010).
  - [65] A. Bérut, A. Arakelyan, A. Petrosyan, S. Ciliberto, R. Dillenschneider, and E. Lutz, Experimental verification of Landauer's principle linking information and thermodynamics, *Nature (London)* **483**, 187 (2012).
  - [66] E. Roldán, I. A. Martínez, J. M. R. Parrondo, and D. Petrov, Universal features in the energetics of symmetry breaking, *Nat. Phys.* **10**, 457 (2014).
  - [67] J. V. Koski, V. Maisi, T. Sagawa, and J. P. Pekola, Experimental observation of the role of mutual information in the nonequilibrium dynamics of a Maxwell demon, *Phys. Rev. Lett.* **113**, 030601 (2014).
  - [68] J. V. Koski, V. F. Maisi, J. P. Pekola, and D. V. Averin, Experimental realization of a Szilard engine with a single electron, *Proc. Natl. Acad. Sci. U.S.A.* **111**, 13786 (2014).
  - [69] J. V. Koski, A. Kutvonen, I. M. Khaymovich, T. Ala-Nissila, and J. P. Pekola, On-Chip Maxwell's Demon as an Information-Powered Refrigerator, *Phys. Rev. Lett.* **115**, 260602 (2015).
  - [70] M. D. Vidrighin, O. Dahlsten, M. Barbieri, M. S. Kim, V. Vedral, and I. A. Walmsley, Photonic Maxwell's Demon, *Phys. Rev. Lett.* **116**, 050401 (2016).
  - [71] J. Goold, M. Huber, A. Riera, L. del Rio, and P. Skrzypczyk, The role of quantum information in thermodynamics—A topical review, *J. Phys. A* **49**, 143001 (2016).
  - [72] J. P. S. Peterson, R. S. Sarthour, A. M. Souza, I. S. Oliveira, J. Goold, K. Modi, D. O. Soares-Pinto, and L. C. Céleri, Experimental demonstration of information to energy conversion in a quantum system at the Landauer limit, *Proc. R. Soc. A* **472**, 20150813 (2016).
  - [73] L. Mancino, M. Sbroscia, E. Roccia, I. Gianani, F. Somma, P. Mataloni, M. Paternostro, and M. Barbieri, Information-thermodynamics of Quantum Generalized Measurements, *arXiv:1702.07164v1* (2017).
  - [74] M. A. Ciampini, L. Mancino, A. Orioux, C. Vigliar, P. Mataloni, M. Paternostro, and M. Barbieri, Experimental extractable work-based multipartite separability criteria, *npj Quantum Inf.* **3**, 10 (2017).
  - [75] N. Cottet, S. Jezouin, L. Bretheau, P. Campagne-Ibarcq, Q. Ficheux, J. Anders, A. Auffèves, R. Azouit, P. Rouchon, and B. Huard, Observing a quantum Maxwell demon at work, *PNAS* **114**, 7561 (2017).
  - [76] Y. Masuyama, K. Funo, Y. Murashita, A. Noguchi, S. Kono, Y. Tabuchi, R. Yamazaki, M. Ueda, and Y. Nakamura, Information-to-work conversion by Maxwell's demon in a superconducting circuit quantum electrodynamical system, *Nat. Comm.* **9**, 1291 (2018).
  - [77] M. Naghiloo, J. J. Alonso, A. Romito, E. Lutz, and K. W. Murch, Information gain and loss for a quantum Maxwell's demon, *arXiv:1802.07205* (2018).
  - [78] Z. Gong and H. T. Quan, Jarzynski equality, Crooks fluctuation theorem, and quantum work statistics, *Phys. Rev. Lett.* **119**, 080601 (2017).

- tuation theorem, and the fluctuation theorems of heat for arbitrary initial states, *Phys. Rev. E* **92**, 012131 (2015).
- [79] S. Rana, S. Lahiri, and A. M. Jayannavar, Quantum Jarzynski equality with multiple measurement and feedback for isolated system, *Pramana* **79**, 233 (2012).
  - [80] F. Liu, Derivation of quantum work equalities using a quantum Feynman-Kac formula, *Phys. Rev. E* **86**, 010103(R) (2012).
  - [81] F. Liu, Equivalence of two Bochkov-Kuzovlev equalities in quantum two-level systems, *Phys. Rev. E* **89**, 042122 (2014).
  - [82] E. P. Wigner, *Group Theory and its Application to the Quantum Mechanics of Atomic Spectra*, translation from German by J. J. Griffin. (Academic Press Inc., New York, 1959).
  - [83] A. Messiah, *Quantum Mechanics* (North Holland Publishing Company, Amsterdam, 1962), Vol 2.
  - [84] L. E. Ballentine, *Quantum Mechanics A Modern Development*, (World Scientific Publishing Co. Pte. Ltd., Singapore, 2000) reprint.
  - [85] F. Haake, *Quantum Signatures of Chaos*, (Springer, Heidelberg, 2010) 3rd edition.
  - [86] P. Talkner, E. Lutz, and P. Hänggi, Fluctuation theorems: Work is not an observable, *Phys. Rev. E* **75**, 050102 (2007).
  - [87] P. Talkner and P. Hänggi, The Tasaki-Crooks quantum fluctuation theorem, *J. Phys. A: Math. Theor.* **40**, F569 (2007).
  - [88] D. Andrieux and P. Gaspard, Quantum Work Relations and Response Theory, *Phys. Rev. Lett.* **100**, 230404 (2008).
  - [89] M. Campisi, P. Talkner, and P. Hänggi, Quantum Bochkov-Kuzovlev work fluctuation theorems, *Philos. Trans. Royal Soc. A* **369**, 291 (2010).
  - [90] B. P. Venkatesh, G. Watanabe, and P. Talkner, Transient quantum fluctuation theorems and generalized measurements, *New J. Phys.* **16**, 015032 (2014).
  - [91] G. Watanabe, B. P. Venkatesh, P. Talkner, M. Campisi, and P. Hänggi, Quantum fluctuation theorems and generalized measurements during the force protocol, *Phys. Rev. E* **89**, 032114 (2014).
  - [92] M. Campisi, P. Talkner, and P. Hänggi, Influence of measurements on the statistics of work performed on a quantum system, *Phys. Rev. E* **83**, 041114 (2011).
  - [93] M. Campisi, P. Talkner, and P. Hänggi, Fluctuation Theorems for Continuously Monitored Quantum Fluxes, *Phys. Rev. Lett.* **105**, 140601 (2010).
  - [94] J. M. Horowitz and S. Vaikuntanathan, Nonequilibrium detailed fluctuation theorem for repeated discrete feedback, *Phys. Rev. E* **82**, 061120 (2010).
  - [95] K. Micadei, J. P. S. Peterson, A. M. Souza, R. S. Sarthour, I. S. Oliveira, G. T. Landi, T. B. Batalhão, R. M. Serra, and E. Lutz, Reversing the thermodynamic arrow of time using quantum correlations, *arXiv:1711.03323* (2017).
  - [96] J. P. S. Peterson, T. B. Batalhão, M. Herrera, A. M. Souza, R. S. Sarthour, I. S. Oliveira, and R. M. Serra, Experimental characterization of a spin quantum heat engine, *arXiv:1803.06021* (2018).